Repression of varicella zoster virus gene expression during quiescent infection in the absence of detectable histone deposition

Jiayi Wang[1], Nadine Brückner[1], Simon Weißmann[2], Thomas Günther[2], Shuyong Zhu[1,3], Carolin Vogt[1,4], Guorong Sun[1], Renzo Bruno[1], Birgit Ritter[1], Lars Steinbrück[1], Benedikt B. Kaufer[5], Daniel P. Depledge[1,3,4], Adam Grundhoff[2] and Abel Viejo-Borbolla[1,3*]

[1] Institute of Virology, Hannover Medical School, Hannover, Germany

[2] Leibniz Institute of Virology, Hamburg, Germany

[3] Excellence Cluster 2155 RESIST, Hannover Medical School, Hannover 30625, Germany

[4] German Center for Infection Research (DZIF), partner site Hannover-Braunschweig, Hannover, Germany

[5] Institute for Virology, Freie Universität Berlin, Berlin, Germany

*Corresponding author

Email: viejo-borbolla.abel@mh-hannover.de

Abstract

Varicella zoster virus (VZV) is a human-specific herpesvirus that establishes latency in peripheral neurons. The only transcripts detected in infected human trigeminal ganglia (TG) obtained shortly after death correspond to the VZV latency-associated transcript (VLT) and associated VLT-ORF63 splice variants. *In vitro* studies showed that VLT-ORF63 is translated into a protein (pVLT-ORF63) that induces VZV transcription. The mechanisms that lead to this restricted gene expression and the transition to lytic replication remain unknown, partly due to the difficulty of working with human neurons. In this study, we addressed whether the neuroblastoma-derived cell line SH-SY5Y could serve as a model to investigate the mechanisms that lead to repression of VZV gene expression followed by reactivation. VZV productively infected differentiated SH-SY5Y (dSH-SY5Y) whereas incubation with acyclovir (ACV) inhibited virus replication and induced a progressive repression of the virus. Upon removal of ACV there was production of viral particles in a subset of cells, while others contained non-replicating VZV genomes and VLT-containing transcripts for at least 20 days post-infection (dpi). Exogenous expression of VLT-ORF63 induced productive infection, suggesting that the non-replicating and repressed genomes remained functional. Interestingly, histone deposition was undetectable at VZV genomes in quiescently infected dSH-SY5Y cells, pointing to a potential novel mechanism leading to VZV repression in this neuronal setting.

Introduction

Varicella zoster virus (VZV) is a highly prevalent human pathogen that causes varicella during primary infection and herpes zoster upon symptomatic reactivation. A large percentage of elderly individuals also suffer post-herpetic neuralgia [1, 2], the second most common type of neuropathic pain worldwide [3]. Moreover, VZV can also cause pneumonia, encephalitis, meningitis and vasculitis in some individuals [4, 5].

VZV establishes latency in neurons of the peripheral nervous system and VZV DNA is detected in approximately 2-5% of sensory neurons in human trigeminal ganglia (TG), with an average of 5-7 copies of the viral genome per infected neuron [6-9]. Epidemiological data and clinical studies suggest that the virus can also establish latency and reactivate in autonomic neurons [10, 11].

VZV latency is characterized by the persistence of the viral genome as an episome, restricted viral transcription, and the capacity of the virus to reactivate, leading to the production of new virions [12]. The VZV latency transcript (VLT) is the only consistently detected VZV transcript in human TGs obtained at short post-mortem intervals. Several TGs also contain VLT splice variants that incorporate the open reading frame 63 (ORF63) sequence (VLT-ORF63) [13, 14]. VLT is encoded antisense to ORF61, the VZV homolog of herpes simplex virus (HSV) infected cell polypeptide 0 [13]. *In vitro* studies with VZV-latently infected human induced pluripotent stem cell (iPSC)-derived neurons (termed HSN) confirmed the expression of VLT during latency, while VLT-ORF63

transcripts were only detected following the incubation of the cells with reactivation stimuli [14]. Translation of VLT-ORF63-1 results in a protein (pVLT-ORF63) that induces widespread VZV gene expression *in vitro* [14]. These results suggest that VLT-ORF63 plays a role during reactivation rather than latency.

The cellular and viral processes leading to VZV latency and reactivation are still unclear. In particular, the kinetics and mechanisms of VZV genome repression are not known. Foetal human neurons have been employed to study VZV neuropathogenesis *ex vivo* or xenotransplanted in severe combined immunodeficiency (SCID) mice [4, 15, 16]. Access to these human cells is scarce, and not permitted in certain countries, complicating their use as a model in many laboratories. As an alternative, human neurons can be derived from embryonic and adult stem cells as well as from iPSCs to study VZV latency and reactivation [17]. Human stem cell-derived neurons treated with acyclovir (ACV) one day prior to infection and infected with low multiplicity of infection (MOI) in the presence of ACV during 6 days support quiescent VZV infection [18]. A similar model had been established for HSV by Wilcox and Johnson and is widely employed to study HSV latency and reactivation, with variations in the exposure time to ACV [19-25].

In an alternative model, infection of stem cell-derived human neurons through the axonal end resulted in a phenotype reminiscent of latency [18]. Interestingly, both models showed a similar phenotype, characterized by very low genome-

wide viral gene expression, no detectable protein translation and no viral particle production. The axonal model of infection was also employed to determine other aspects of VZV latent infection, including the reactivation potential of the vaccine Oka strain and the expression profile of the VZV latency transcript (VLT) *in vitro* [14, 26].

The derivation of human neurons from stem cells is expensive and time consuming. In addition, it is difficult to obtain sufficient neuronal cells for mechanistic experiments and to study the kinetics of VZV gene repression during establishment of latency. Furthermore, the obtained neuronal cultures tend to be heterogenous [27-30] and the starting precursor culture and the differentiation method employed determine the percentages and types of derived neuronal cells [31]. There is thus an unmet need for an expandable neuron-like model that allows the study of VZV repression and reactivation.

To address this, we here examined the utility of the SH-SY5Y cells for the study of VZV repression prior to the establishment of latency. SH-SY5Y is a subclone of a neuroblastoma cell line obtained from a bone marrow biopsy [32]. SH-SY5Y cells can be differentiated into mature neuron-like cells by different protocols and are commonly employed to study neurological processes and diseases [33-35]. They have also been employed to study the neurotropism of several viruses including VZV [36, 37], HSV and HSV-derived vectors [38, 39] and human cytomegalovirus [40]. While laboratory adapted and clinical VZV

strains productively infect differentiated SH-SY5Y cells (dSH-SY5Y) [36, 37], latent infection and reactivation has not been studied with these cells.

Here we established a model to study VZV repression and de-repression employing dSH-SY5Y cells. Our results suggest that a progressive repression of VZV gene expression occurs upon ACV incubation. Non-replicating viral genomes and transcripts from the VLT locus were detected in a small percentage of dSH-SY5Y cells up to 20 days post-infection (dpi). Ectopic expression of pVLT-ORF63 induced productive VZV infection. Interestingly, the bulk of VZV genomes in non-productively infected cells were not occupied by histone H3. Despite the apparent absence of repressive chromatin, however, we found only a subfraction of genomes to be in an accessible state, a finding which was in accord with the observed low levels of transcripts throughout the viral genome and the absence of detectable viral protein and virus production. These results, together with the expandable nature and robust differentiation of SH-SY5Y provide an opportunity to study the mechanisms leading to VZV repression and de-repression in human neuron-like cells.

Results

Differentiation of SH-SY5Y cells into neuron-like cells

Non-differentiated SH-SY5Y cells contain a mixture of neuronal and epithelial precursor cells. To obtain differentiated SH-SY5Y (dSH-SY5Y) cells with characteristics of human neurons, we modified a successful differentiation method [41]. A schematic representation of the protocol is shown in Figure 1A. The main modification from the original protocol was the detachment of neuron-like cells with collagenase followed by seeding onto Matrigel-coated plates, while the epithelial-like cells remained attached onto the original well.

After 18 days of differentiation, the dSH-SY5Y neuron-like cells had a smaller cell body than the original cells and long, branched neurite projections connecting with the surrounding cells (Fig 1B). Furthermore, from 18 days post differentiation (dpd), the dSH-SY5Y cells expressed several proteins found in mature neurons, including microtubule-associated protein 2 (MAP2), β-III-tubulin (Tuj1), Nav 1.7, and dopamine beta hydroxylase (DBH) (Fig 1C). We did not detect DAPI positive cells lacking neuronal markers, suggesting that the majority of cells had a neuron-like phenotype. We then tested whether dSH-SY5Y cells underwent active mitosis by performing KI67 staining. In undifferentiated SH-SY5Y cells, 56% of the cells were KI67 positive. This reduced to 14% at 12 dpd, 3% at 20 dpd, and 1% at 30 dpd (Fig 1D), indicating that dSH-SY5Y cells were predominantly post-mitotic at 20 dpd.

These results indicate that the modified protocol resulted in successful neuronal differentiation of SH-SY5Y cells.

VZV reporter virus replicates efficiently in neuron-like SH-SY5Y cells

To follow the infection and spread of VZV in dSH-SY5Y cells, we employed a recombinant bacterial artificial chromosome (BAC) VZV pOka strain [42] expressing RFP fused to immediate early ORF63 and GFP fused to the leaky-late gene ORF11 (termed v63R/11G, Fig 2A). The expression of the fluorescent proteins allowed us to observe the progression of VZV productive infection.

We infected dSH-SY5Y cells with cell-free v63R/11G at an MOI of 0.001, and detected RFP and GFP positive cells at 3, 5 and 12 dpi. The number of RFP and GFP positive cells increased over time (Fig 2B). Similarly, the viral genome copy number increased from an average of 2 copies per cell at 1 dpi to an average of 50 copies per cell at 6 dpi (Fig 2C). The transcripts of immediate early genes ORF4 (IE4), ORF61 (IE61) and early gene ORF68 (glycoprotein E, gE) [43] also increased over time (Fig 2D-F). These results showed that v63R/11G efficiently replicates in dSH-SY5Y, in line with previous observations [36, 37].

The duration of ACV incubation determines the level of repression of VZV gene expression in dSH-SY5Y cells

A previous study showed that pretreatment of human stem cell-derived neurons with ACV for 24 hours followed by low MOI VZV infection in the presence of ACV for 6 days leads to a phenotype reminiscent of latency [18]. Therefore, we employed the same procedure in an attempt to establish VZV quiescent infection and reactivation in dSH-SY5Y cells. We also employed different ACV incubation times to determine whether this would impact VZV repression. We pretreated dSH-SY5Y cells for 24 hours with ACV and then infected them at an MOI of 0.001 in the presence of the drug during 2, 3, 4, 5 or 6 dpi (Fig 3A). We monitored the cells twice a day for 30 dpi to detect ORF63-RFP and ORF11-GFP expression, indicative of productive VZV replication. We observed a negative correlation between the number of days the infected-cells were incubated with ACV and the time post-ACV removal when ORF63-RFP- and ORF11-GFP-positive cells were detected (Fig 3B, C). At 30 dpi, only 1 well (1.4% of wells) had ORF63-RFP- and ORF11-GFP-positive cells when cells had been incubated with ACV for 6 dpi. However, this increased to 45.7% of wells in cells incubated with ACV for 5 dpi. These results indicated that the time of ACV incubation positively correlates with the duration of VZV inhibition.

Incubation with ACV for 5 days results in a repressive phenotype that can be spontaneously reversed

We next focused on dSH-SY5Y cells incubated with ACV for 5 dpi (Fig 4A). The samples containing cells expressing ORF63-RFP and ORF11-GFP have

193 replicating VZV and were termed “R”, while those lacking the fluorophores were
194 termed “NR”. The expression of ORF63-RFP and ORF11-GFP also correlated
195 with the presence of VZV gE (Fig 4C).
196 We quantified the expression of *ORF61* and *ORF68* during acute infection as
197 well as at several dpi following incubation with ACV in samples lacking
198 detectable ORF63-RFP and ORF11-GFP (Fig 4D, E). We also analyzed cells
199 expressing ORF63-RFP and ORF11-GFP at different days post-release of
200 repression (dpr) by ACV. The expression of both *ORF61* and *ORF68* was
201 higher during acute infection than in the other conditions and it increased with
202 time, indicating productive viral replication and virus spread. By contrast, the
203 expression of both genes was very low in the presence of ACV and following
204 ACV removal. The viral gene expression in wells that contained ORF63-
205 RFP/ORF11-GFP positive cells, indicative of VZV replication, was 10-20 times
206 higher than in those lacking ORF63-RFP/ORF11-GFP positive cells but lower
207 than in acute infection, and also increased with time (Fig 4D,E).
208 We also quantified VZV genome copy numbers as a surrogate of VZV
209 replication (Fig 4F). The number of viral genomes increased in the cells infected
210 without ACV, while in those exposed to ACV for 5 days, the level of viral
211 genomes decreased with time. To determine whether cells lacking detectable
212 ORF63-RFP and ORF11-GFP expression contained the viral genome, we
213 performed *in situ* hybridization (DNAscope) in wells lacking detectable
214 expression of these fluorophores and detected VZV DNA (VLT locus) at 12 and

20 dpi. The virus genome was detected in about 5% of the cells that were incubated with ACV for 5 days (Fig 4G). The low number of viral genomes detected by *in situ* hybridization combined with qPCR results, suggest that there was no ongoing viral replication in these cells.

Finally, seeding of dSH-SY5Y cells expressing ORF63-RFP and ORF11-GFP on top of ARPE19 cells led to productive infection of these epithelial cells (Fig 4H), demonstrating the presence of infectious viral particles. These results suggest that incubation with ACV for 5 days leads to two phenotypes, one characterized by cells containing viral genomes that produce infectious virus and another one by cells that maintain non-replicating viral genomes.

Less than 5% of dSH-SY5Y cells incubated with ACV during 6 days maintain non-replicating viral genomes for at least 30 dpi

The presence of ACV 1 day prior to VZV infection and during 6 dpi led to a near complete repression of VZV, with 98.6% of VZV infected wells containing cells lacking ORF63-RFP and ORF11-GFP expression for up to 30 days (Fig 3C and Fig 5A, B). Similarly, we could not detect viral proteins gE and IE4 by WB at different dpi following 6 days incubation with ACV (Fig 5C). The expression of VZV *ORF4*, *ORF61* and *ORF68* was much lower in ACV incubated cells than in acute infected cells at 6 dpi and decreased further over time following ACV removal (Fig 5D-F). We detected viral DNA by qPCR in the inoculated wells at

6, 12, 16, 20 and 30 dpi, with DNA copy numbers consistently averaging 1 genome copy or less per cell (Fig 5G).

We detected VZV DNA (VLT locus) at 12 and 20 dpi in about 4.4% of cells that were incubated with ACV for 6 days (Fig 5H). These results suggested that a low number of dSH-SY5Y cells infected with VZV in the presence of ACV for 6 dpi maintain VZV genomes with very low gene expression, lack of detectable protein and virus production, potentially reflecting a quiescent state.

We repeated these experiments with a BAC-derived pOka strain VZV expressing GFP instead of ORF57 (pOka-Δ57-GFP, Supplementary Figure 1 and not shown). This virus was previously generated (Accession number PP378487; [44]). We obtained similar repression of VZV in the presence of ACV for 6 days, suggesting that the obtained results were not strain specific.

Ectopic VLT-ORF63 expression induces VZV replication and virus production in infected dSH-SY5Y cells incubated with ACV for 6 days

We next examined whether addition of drugs previously used as reactivation stimuli could induce de-repression of VZV after 6 days incubation with ACV. We tested LY294002, an inhibitor of phosphoinositide 3-kinase (PI3K) and suberanilohydroxamic acid (SAHA), an inhibitor of histone deacetylases, at 8 dpi (2 days after removal of ACV) (Fig 6A). LY294002 has been previously shown to induce VZV reactivation [18], while SAHA induces reactivation of Kaposi's sarcoma-associated herpesvirus (KSHV) [45]. Incubation with LY or

SAHA slightly increased VZV gene expression without detectable ORF63-RFP and ORF11-GFP protein, lack of infectious virus, and led to cell death after 4 days of incubation (Fig 6B,C).

Ectopic VLT-ORF63 expression induced transcription of VZV IE, E, and L genes in latently VZV-infected HSN, suggesting that the pVLT-ORF63 fusion protein is involved in the transition from latency to lytic infection [14]. Therefore, we addressed whether the ectopic expression of VLT-ORF63 could induce VZV reactivation and production of infectious virus in the dSH-SY5Y cells infected in the presence of ACV for 6 days. We incubated quiescently infected dSH-SY5Y cells with SAHA and LY294002, or transduced them with lentiviruses expressing VLT-ORF63 or GFP (Supplementary Figure 2). The VLT-ORF63 lentivirus induced VZV protein expression and virus spread, monitored by ORF63-RFP and ORF11-GFP positive cells in about half (21/41) of the wells (Figure 6D,E), while the eGFP control lentivirus or the treatment with SAHA and LY did not (Figure 6B,C and data not shown).

A single nitrocellulose membrane was used to detect protein expression sequentially (Supplementary Figure 3, blots on left side). VLT-ORF63 or ORF63-RFP proteins were detected in acutely infected cells, in “NR” (probably expressed from the VLT-ORF63 lentivirus) and “R” samples. ORF63, gE and ORF11-GFP were detected only in acutely infected cells and “R” samples, while eGFP was also observed in cells transduced with eGFP control lentivirus. Considering the similar size of VLT-ORF63 and ORF63-RFP proteins, another

nitrocellulose membrane loaded with the same samples was incubated with an anti-RFP antibody to confirm the expression of ORF63-RFP in acutely infected cells and “R” samples (Supplementary Figure 3, blots on right side).

These results show that pVLT-ORF63 releases the repression on the VZV genome in dSH-SY5Y cells incubated with ACV for 6 days, highlighting that the infection was not abortive.

Incubation with ACV leads to low level genome-wide VZV transcription in infected dSH-SY5Y cells

We next analyzed the VZV transcriptome in dSH-SY5Y cells infected in the presence of ACV during 3, 4, 5 and 6 dpi at different times post-ACV removal. We detected transcripts across the VZV genome, although of low magnitude (Fig 7A, B). The expression level negatively correlated with ACV incubation time. Whether any of these transcripts corresponds to mature RNA that could be translated is unknown at present. We detected transcription across the VLT exons in acutely infected cells and at 2 days post-ACV removal following 5 and 6 days incubation with ACV (Supplementary Figure 4). VZV genome-wide expression was also reported when infecting human stem cell-derived neurons in the presence of ACV or through the axonal end [18, 26]. We also performed RNA *in situ* hybridization (RNAscope) with a probe that binds VLT and VLT-ORF63 transcripts [14] and detected these transcripts in the cytoplasm of about 1% of dSH-SY5Y cells at 12 and 20 dpi (following incubation with ACV for 6

302 days) (Fig 7C). This corresponds to about 20-25% of cells containing the viral
303 genome. These results suggest that a small number of dSH-SY5Y cells
304 maintained the viral genome without active replication and expressing VLT or
305 VLT-ORF63.
306
307 **Only a minority of VZV genomes in quiescently infected dSH-SY5Y cells**
308 **are accessible while the bulk of genomes lack detectable histone**
309 **deposition**
310 We performed ChIP-seq and ATAC-seq analyses of ACV-treated dSH-SY5Y
311 cells 13 days after infection to elucidate the chromatin status of resident VZV
312 genomes. These experiments were performed with v63R/11G and the parental
313 BAC-derived pOka strain lacking any fluorophores (termed WT, [42]). Mapping
314 to the human genome confirmed the fidelity and functionality of reagents and
315 experimental protocols. As examples, the top and center panels in Figure 8
316 show coverage tracks of two regions on chromosome 17 and 19 that
317 encompass loci enriched for facultative and constitutive heterochromatin marks
318 (H3K27me3 and H3K9me3, respectively), but also contain euchromatic
319 promoter regions decorated by activation-associated H3K3me3 and H3K27ac
320 marks. Figure 8B shows average read densities of ChIP-seq and ATAC-seq
321 samples across all annotated human transcriptional start sites (TSS). As
322 expected, H3K27ac and H3K4me3 signals were strongly enriched in the +/- 2.5
323 kb flanking regions, with locally decreased coverage indicative of a

nucleosome-free region at the TSS in the center. Conversely, ATAC-seq densities exhibited marked peaks flanking the position of the +1 nucleosome. Surprisingly, although VZV was highly covered by input reads, we did not observe any significant histone modification patterns across the viral genome (lower panel in Figure 8A). Indeed, when compared to input and the host genome, pan-H3 ChIP-seq coverage was also very low, suggesting that most viral genomes lack canonical chromatin. In support of this notion, Figure 8C shows a relative enrichment analysis of the viral genome compared to positive and negative host regions for each of the analyzed histone marks. For this purpose, we determined average ChIP-seq signals by calculating enrichment in the most significantly called host peak regions (positive control regions, left panel) relative to a set of randomly selected negative host regions (set to one; center panel) and compared these to input-normalized values from windows shifted across the viral genome (right panel). As anticipated, the magnitude of positive control ChIP-signals varied between individual antibodies, with the greatest and lowest values observed for the H3K4me3 and pan-H3 antibodies, respectively (note that low signals are to be expected for pan-H3, as overall nucleosome density does not exhibit high variability across host regions). As shown in the right panel, ChiP-seq signals in the viral genome were consistently below one (i.e., the value assigned to the negative control regions), likely reflecting the fact that histone-free genomes do not elicit either specific or unspecific signals and contribute to input only.

In contrast to ChIP-seq, ATAC-seq produced appreciable coverage across the entire viral genome (bottom panel and track in Figure 8A). Nevertheless, quantitative analyses of input-normalized ATAC-seq signals demonstrates that viral ATAC-seq signal levels, though significantly above background (p=1.2E-48, one-sided heteroscedastic t-test), reach only 6% of those seen in positive host regions (Fig. 8D). This observation suggests that, although the bulk of viral genomes is not decorated by histones, only a subset of them is accessible to Tn5 transposase in ATAC-seq assays. Since we obtained similar results with pOka and v63R/11G, our results indicate that the obtained results are not strain specific.

Discussion

How neuronal cells repress and regulate VZV gene expression prior to and during latency and how this repression is released upon reactivation is not known. This is partly due to the difficulty of performing experiments such as ChIP-seq that require large number of cells with human neuronal models that support latency and reactivation. Here, we attempted to establish a human neuronal model with dSH-SY5Y cells to investigate how VZV is repressed and maintained in a quiescent state.

dSH-SY5Y cells are commonly employed in neurobiological research [46-48], in neuroinfection [36, 37, 49, 50] and support full VZV replication and cell-to-cell spread [36, 37, 51], but a quiescent state has not been previously reported. Differentiation of SH-SY5Y cells was successful as shown by the expression of neuronal markers, as well as by lack of cell division. Two different recombinant VZV replicated and spread in dSH-SY5Y, in line with previous reports [36, 37, 52]. We employed ACV to establish a non-productive infection as previously done with stem cell-derived neurons [18]. Longer ACV incubation times drastically reduced the frequency of productive replication after ACV removal. These results, together with the progressive reduction in gene expression across the whole VZV genome upon removal of ACV, suggest that following VZV entry in dSH-SY5Y cells, there was a progressive repression of viral gene expression that correlated with the duration of ACV treatment. One interesting observation was the different phenotype when cells were treated with ACV for

5 days in comparison with 6 days. Incubation with ACV for 5 dpi repressed VZV but allowed spontaneous de-repression in about half of the wells following removal of the drug. In contrast, repression after 6 days of ACV treatment was nearly complete, with only 1.4% of wells containing productively infected cells at 30 dpi.

Approximately 4.4% of individual neuron-like cells treated with ACV for 6 dpi retained the viral genome for at least 20 dpi. The fact that only one copy of the genome was normally detected in these cells suggests that there was no DNA replication and the infection could be abortive. However, about 1% of these repressed cells – corresponding to approximately 20-25% of cells harboring the genome – expressed transcripts across VLT exons at 12 and 20 dpi. Since the RNAscope probe employed detects both VLT and VLT-ORF63 transcripts, we cannot conclude which one is expressed in these neuron-like cells. However, these results suggest the establishment of restricted gene expression in a reduced number of dSH-SY5Y cells and indicate that the infection in the presence of ACV during 6 days was not abortive, at least in these cells. This was supported by the production of infectious virus upon exogenous expression of VLT-ORF63.

We also observed a reduction in the level of viral gene expression over time when analyzing the VZV transcriptome. The transcriptome profile of VZV in dSH-SY5Y cells incubated with ACV was similar to that of acutely infected cells, although with much lower expression. Previous results employing stem cell-

derived neurons also found that following ACV incubation, or upon axonal infection, the transcription profile of VZV did not mirror the transcriptome obtained in human TG following decades of latent infection [18, 26]. In these reports the expression of VLT was not investigated since this transcript had not been discovered yet [13]. In another report, axonal infection of human iPSC-derived neurons with cell-free VZV pOka strain led to expression of VLT and non-detectable expression of ORF63 by RT-qPCR, suggesting that a latent phenotype was achieved, although the genome-wide transcription profile of VZV was not analyzed [14].

As has been shown for HSV [53, 54], regulation of VZV latency is probably mediated by a combination of immune and epigenetic mechanisms. We hypothesized that repressive histone modifications were responsible for the phenotypes observed after long-term ACV incubation in dSH-SY5Y cells. Surprisingly, however, we could not detect any significant enrichment of histones (H3 and modifications as well as H2AK119Ub) on the viral genome of infected dSH-SY5Y cells treated with ACV during 13 days. These results were obtained with two different recombinant VZV, the parental pOka and v63R/11G, indicating that they were not due to the modification of the viral genome. Our observations strongly suggest that the bulk of VZV genomes in ACV-treated cells are nucleosome-free and consequently cannot be silenced by transcriptional repressors recruited via histone marks. Nevertheless, considering that only a small proportion of viral genomes produced ATAC-seq

signals, we suspect that repression may, at least in part, be the consequence of reduced accessibility of viral genomes to transcription factors and/or the transcriptional machinery. While the underlying mechanisms will doubtlessly require further investigation, we consider sequestration or entrapment of genomes in sub-nuclear compartments such as, for example, phase-separated PML bodies or stalled replication compartments as potentially contributing factors.

There is also the possibility that at least some of the persisting VZV genomes may be partially or fully protected by capsid proteins, e.g., in virions trapped at the nuclear envelope or in PML bodies [55, 56]. Likewise, it is possible that histone-independent recruitment of repressors such as IFI16 or SMC5/6 could contribute to transcriptional repression, as shown for other viruses including HSV-1 [57-62]. Another confounding factor could be DNA methylation, although this epigenetic mark does not seem to be relevant during HSV-1 latency [63, 64]. Apart from the presumably inactive genomes, we also do not know to what extent the minority of VZV genomes that are accessible in ATAC-seq assays contribute to the observed phenotypes. Since these genomes appear to be globally accessible, it is tempting to speculate that they may represent the source of the observed low-level genome-wide transcription patterns. However, at present we also cannot exclude the possibility that transcription originates from a very small subfraction of chromatinized genomes that is below the detection limit of our ChiP-seq assays.

Therefore, more research is warranted to understand how VZV is repressed upon infection of neuronal cells.

Overall, our results suggest that dSH-SY5Y could be employed to investigate the initial steps that lead to repression, persistence and reactivation of the VZV genome. Moreover, they point to the existence of potentially novel mechanisms involved in VZV repression.

Materials and methods

Cells and virus

Neuroblastoma-derived SH-SY5Y (ATCC-CRL-2266) and epithelial ARPE19 (ATCC-CRL-2302) cells were maintained in a humidified incubator at 37 °C with 5% CO_2. Undifferentiated SH-SY5Y cells were cultured in DMEM/Nutrient mixture F-12 Ham medium (Sigma) with 15% Fetal bovine serum (Sigma), supplemented with penicillin–streptomycin (Cytogen) and L-glutamine (Cytogen). ARPE19 cells were cultured in DMEM/Nutrient mixture F-12 Ham medium with 8% FBS, supplemented with penicillin–streptomycin and L-glutamine.

Generation of fluorescent reporter viruses

We previously fused the monomeric red fluorescent protein (mRFP) to the C-terminus of ORF63/70 in the pOka bacterial artificial chromosome system (BAC) (pP-Oka) [42] and could show that it is expressed in persistently infected neuronal cells [65, 66]. To visualize productively infected cells, we fused eGFP to the C-terminus of ORF11 (UL47), a tegument protein that is only expressed during lytic replication, using two-step Red-mediated en passant mutagenesis [67, 68], Recombinant BAC clones were confirmed by PCR, DNA sequencing and RFLP using different restriction enzymes to ensure integrity of the virus genome. The recombinant virus was reconstituted by transfection of BAC DNA into MeWo cells as described previously [42, 69].

Cell-free VZV preparation

Monolayers of ARPE19 cells growing in P150 dishes were used to prepare cell-free virus. ARPE19 cells were infected with the VZV cell debris or cell-associated virus. Cell-free virus was prepared when about 80% of cells were RFP positive. The infected ARPE19 cells were washed with ice-cold PBS and then detached by scraping in ice-cold PSGC (PBS containing 5% sucrose (Roth), 0.1% monosodium-glutamate (Sigma) and 10% FCS) buffer (5 ml PSGC buffer/ P150 dish). The cells were transferred into 50 ml tubes and sonicated on ice 3 times for 15 seconds with a 15 second interval with a Bandelin Sonorex RK100 sonicator. Then, the cells were centrifuged for 15 minutes at 1000 *g* at 4 °C. The supernatant was transferred to a new 50 ml tube and mixed with ice-cold Lenti-X concentrator (ratio Lenti-X:supernatant = 1:4 or 1:3). The mixture was incubated at 4 °C for 2-3 hours, followed by centrifugation at 1,500 *g* at 4 °C for 45 min and removal of the supernatant. The cell pellet containing 10-fold concentrated cell-free virus was resuspended and aliquoted in ice-cold PSGC buffer and stored at -80 °C.

Titration of VZV

The determination of 50% tissue culture infection dose (TCID50) based on Spearman-Karber method was used to determine the virus titer. To this end, ARPE19 cells at a confluency of about 70% in 96 well plates (~ 10^4 cells per well) were infected with serial dilutions of cell-free VZV. Cell-free VZV stocks

were thawed in a 37 °C water bath and 10-fold serial dilutions were prepared in DMEM/F12 medium containing 2% FBS. For each viral dilution factor, 8 wells in a 96 well plate were inoculated with 100 µL/well and infection was assessed by RFP and GFP expression. The inoculum was maintained for 6 days, when the number of wells containing RFP and GFP expression was counted, and the VZV titer was calculated according to the Spearman-Karber formula:

log10 TCID50= -(X0-d/2+d/n*ΣXi).

X0= log10 of the reciprocal of the maximum dilution (minimum concentration) where all wells were infected; d= log10 of the dilution factor; n= number of replicates / dilution; Xi= total number of virus-infected wells after X0, including X0. The final titer in plaque forming units per mL (PFU/mL) was calculated using the formula 0.69*TCID50/mL.

Differentiation of SH-SY5Y cells

When SH-SY5Y cells reached approx. 60-70% density in a P100 dish, they were used for differentiation. Two types of differentiation media were used during 18-day differentiation. The cells were cultured in Differentiation Medium #1 (47.7 ml Nutrient Mixture F12 (DMEM F12) (Gibco), 1.3 ml Fetal bovine serum (Sigma), 0.5 ml GlutaMAX supplement (Gibco) and 0.5 ml penicillin–streptomycin (Cytogen)) with 10 µM All-trans retinoic acid (RA) during the first 10 days of differentiation. The medium was replaced every two days. At day 10, the cells were washed with PBS and incubated with 200 U/mL Collagenase

Type IV (Gibco) diluted in DMEM/F-12 GlutaMAX(TM) medium at 37 °C for 5-10 min, until the axons of the neuron-like cells disappeared. The collagenase was gently removed and the edge of the plate was tapped to detach the neuron-like cells, leaving the epithelial-like cells still attached. The detached cells were rinsed with DMEM/F-12 GlutaMAX(TM) medium, transferred into a 50 mL centrifuge tube and centrifuged at 200 *g* for 5 min. The supernatant was removed and the cell pellet was resuspended in Differentiation Medium #2 (47 ml Neurobasal Medium (Gibco), 1 ml B-27 Supplement Minus AO (50X) (Gibco), 20 mM potassium chloride (Carl Roth), 0.5 ml GlutaMAX supplement (Gibco), 0.5 ml penicillin–streptomycin (Cytogen), 1 mM Dibutyryl-cAMP (dbCAMP) (Selleckchem), 20 ng/mL recombinant human brain-derived neurotrophic factor (Peprotech) and 10 ng/mL recombinant human nerve growth factor (Peprotech) containing 10 µM RA. 100,000-150,000 or 50,000-75,000 cells/well were seeded on Matrigel-coated (0.15-0.16 mg/ml; Corning) 12- or 24-well plates, respectively. The cells were cultured in Differentiation Medium #2, which was replaced every two days. From day 18, the dSH-SY5Y cells were used for experiments.

Virus infection and establishment of VZV repression state in dSH-SY5Y cells

dSH-SY5Y neuron-like cells at 18-20 days post-differentiation were employed in infection experiments. For acute infection, dSH-SY5Y cells were incubated

545 with cell-free v63R/11G for 4 h at 37°C using an MOI based on the titer of virus
546 obtained in ARPE19 cells. After 4 h, the virus inoculum was removed, the cells
547 were carefully rinsed 3 times with PBS and Differentiation Medium #2 with 10
548 µM RA was added. To study VZV repression, dSH-SY5Y cells were incubated
549 with Differentiation Medium #2 containing 10 µM RA and 100 µM acyclovir
550 (Acycloguanosine, ACV, Sigma) 24 hours prior to infection. Before infection,
551 the supernatant of dSH-SY5Y containing RA and100 µM ACV was harvested
552 and used as conditioned medium. Neuron-like cells were infected with cell-free
553 v63R/11G in Differentiation Medium #2 containing 100 µM ACV. Mock-infected
554 control dSH-SY5Y cells were incubated in Differentiation Medium #2 containing
555 100 µM ACV and the same volume of PSGC buffer as in the virus preparation
556 used for infection. After 4 hours incubation, dSH-SY5Y cells were carefully
557 rinsed 3 times with PBS and incubated with conditioned medium. Differentiation
558 Medium #2 containing 10 µM RA and 100 µM ACV was changed every two
559 days. To induce virus replication, 10 µM PI3-kinase inhibitor (LY294002,
560 Abcam), 2 µM histone deacetylase (HDAC) inhibitor suberoylanilide
561 hydroxamic acid (SAHA) or lentivirus expressing eGFP or VLT-ORF63 were
562 added at 8 dpi and incubated for 1 - 4 days.
563
564 **Generation of a lentivirus expressing VLT-ORF63**
565 For the lentiviral RRLPPTSF-based VLT63-1 vector, the VLT63-1 cDNA
566 sequence was inserted into the vector using *Age*I and *Bam*HI restriction sites.

For virus production, 5 × 10^6 HEK 293T cells were seeded in a 10-cm dish the day before transfection. Transfections were performed using the calcium phosphate precipitation method with 5 µg RRLPPTSF-pVLT63-1 (or a RRLPPTSF-eGFP control vector [70]), 10 µg gag-pol, and 0.5 µg vsvg (packaging and envelope plasmids). Supernatants were collected 42 h and 48 h after transfection, passed through a 0.22 µm filter (Millipore), and stored at –80°C.

DNA and RNA isolation, cDNA synthesis and quantitative PCR

Total DNA and RNA were isolated from cells using the AllPrep DNA/RNA Mini Kit (Qiagen) according to the manufacturer's instructions. The cDNA was synthesized using the LunaScript™ RT SuperMix Kit (New England Biolabs) in 20 µL reaction containing 4 µL SuperMix (5X) and 1 µg RNA. Relative quantitative PCR (qPCR) and absolute qPCR were performed using a qTOWER³ Real-time Thermal Cycler (Analytik Jena). 2 µL template cDNA/DNA was used in a 20 µL reaction containing 10 µL Luna® Universal qPCR Master Mix (New England Biolabs). The qPCR program was: 1 cycle of 95 °C hot start for 10 min and 45 cycles of 95 °C for 15 s and 60 °C for 45 s. For relative qPCR, viral mRNA was detected from VZV genes ORF4, ORF61, ORF62 and ORF68, human β-actin measured for normalization. For absolute qPCR, VZV ORF63 served as the viral genome target, while human β-actin served as the host genome target for normalization. PCR products were cloned into pGEM-T Easy

589 Vector (Promega) and standard curves were generated using 10-fold serial
590 dilutions (10^2 -10^9) of templates. The copy number of the target gene in the
591 sample was calculated by normalizing to the standard curve. Primer sequences
592 can be found in Table 1 and 2.

Name	Sequence (5'-3')
ORF4_F	GCCCATGAATCACCCTC
ORF4_R	ACTCGGTACGCCATTTAG
ORF61_F	GGACAGACTGCCTTTTCGAG
ORF61_R	GACAACGCAGGGATGTTTTT
ORF68_F	GTACATTTGGAACATGCGCG
ORF68_R	TCCACATATGAAACTCAGCCC
actin_F	TCATCACCATTGGCATGAG
actin_R	AGCACTGTGTTGGCGTACAG

593 Table 1: Sequences of primers used to quantify gene expression

594

Name	Sequence (5'-3')
VZV-ORF63_F	CCCGGCGCGTTTTGTACTCC
VZV-ORF63_R	ACAATTCCTCCCAGCACGCTA
h-β-Actin_F	TCCTCCTGAGCGCAAGTACTCC
h-β-Actin_R	AAGTCATAGTCCGCCTAGAAGCA

595 Table 2: Sequences of primers used to determine genome copy number

596

Western blotting

Cells were lysed using radioimmunoprecipitation assay (RIPA) buffer (Sigma-Aldrich) with Pierce protease inhibitor minitablets (Thermo Fisher Scientific). Lysates were rocked for 20 min at 4 °C and centrifuged at 13,000 rpm at 4 °C for 15 min. Supernatant was collected as total protein. Stain-free total protein detection was performed as previously described [71]. Briefly, protein samples were mixed with SDS loading buffer, heated at 98 °C for 5 min and loaded into SDS-PAGE gels containing 1% 2,2,2-Trichloroethanol (TCE). Total proteins were visualized by illumination with UV light using ChemiDoc MP Imaging System (Bio-Rad). The separated proteins were transferred onto nitrocellulose membranes and then blocked in 5% skimmed milk plus PBS-0.1% Tween 20 (PBS-T). Primary antibodies were diluted in PBS-T containing 5% skimmed milk and incubated overnight at 4 °C. Membranes were then washed 3 times with PBS-T buffer for 10 min and then incubated in PBS-T containing 5% skimmed milk and fluorescently-conjugated secondary antibody for 1 h at room temperature. Membranes were then washed as described above and detection was performed with ChemiDoc MP Imaging System (Bio-Rad). The antibodies were as follows: mouse monoclonal anti-VZV gE (LSBio Biozol, 1:2,000); mouse anti-VZV ORF4 (CapRi, 1:1,000); mouse monoclonal anti-VZV ORF63 Cl.63.08, kappa IgG1 (Capri Center for Proteomics, 1:1,000); mouse monoclonal anti-β-actin (Thermo Scientific, 1:5000); mouse monoclonal anti-

RFP-antibody (3F5) (ChromoTek GmbH, 1:1000); mouse monoclonal anti-GFP (TaKaRa, 1:1000); anti-mouse IgG IRDye 800 (LI-COR, 1:10,000).

Immunofluorescence

Cells were washed with PBS, fixed for 20 min with 4% paraformaldehyde at room temperature, washed again and incubated in permeabilizing and blocking solution (0.5 % Triton X-100, 5 % BSA) for 1 h. Cells were labelled with the following primary antibodies diluted in PBS containing 0.1% Triton X-100, 1% BSA at 4 °C overnight: rabbit anti-microtubule-associated protein 2 (MAP2, Millipore 1: 200); sheep polyclonal anti-dopamine beta hydroxylase (DBH, Thermo Fisher Scientific, 1:50); Tuj1 mouse anti-tubulin-β-III (Tuj1, Millipore, 1:300); rabbit polyclonal anti-Nav 1.7 (Alomone, 1:200); rabbit polyclonal anti-KI67 (Proteintech, 1:400). Cells were then washed, incubated 1 h at room temperature with DAPI and conjugated secondary antibodies: anti-mouse IgG Alexa Fluor 488 (Life Technologies, 1:1000); anti-mouse IgG Alexa Fluor 555 (Life Technologies, 1:1000); anti-sheep IgG Alexa Fluor 488 (Life Technologies, 1:1000). Cells were washed and mounted onto glass slides with Prolong Gold Antifade Mountant (Thermo Fisher). Images were obtained using a Zeiss observer Z1 inverted microscope.

Chromatin Immunoprecipitation (ChIP)

639 ChIP was performed as described previously [72]. Cells were cross-linked (1 %
640 formaldehyde, 10 minutes), quenched with 125 mM glycine, washed twice with
641 PBS and harvested in 1 ml buffer 1 (50 mM Hepes-KOH, 140 mM NaCl, 1 mM
642 EDTA, 10 % glycerol, 0.5 % NP-40, 0.25 % Triton X-100) and incubated for 10
643 min at 4 °C while rotating. After centrifugation (1,350 x g, 5 min), nuclei were
644 incubated with 1 ml buffer 2 (10 mM Tris-HCl, 200 mM NaCl, 1 mM EDTA, 0.5
645 mM EGTA) for 10 min at 4 °C while rotating. Pelleted nuclei were lysed in buffer
646 3 (1 % SDS, 10 mM EDTA, 50 mM Tris-HCl). Chromatin was sonicated
647 (fragment size 200-500 bp) using a Bioruptor™ (Diagenode). After addition of
648 Triton X-100 (1 % final concentration) cell debris was pelleted (20,000 x g, 4°C)
649 and chromatin containing supernatant was collected. Chromatin of $1x10^6$ cells
650 was diluted 1:10 in dilution buffer (0.01 % SDS, 1.1 % Triton X-100, 1.2 mM
651 EDTA, 16.7 mM Tris-HCl, 167 mM NaCl) and incubated with respective
652 antibodies overnight. 50 µl BSA-blocked Protein A/G Magnetic Beads
653 (Pierce™) was added to precipitate the chromatin-immunocomplexes and
654 incubated for 3 hr at 4°C. Beads were washed once with 1 ml of the following
655 buffers: low-salt buffer (0.1 % SDS, 1 % Triton X-100, 2 mM EDTA, 20 mM Tris-
656 HCl, 150 mM NaCl); high-salt buffer (0.1 % SDS, 1 % Triton X-100, 2 mM
657 EDTA, 20 mM Tris-HCl, 500 mM NaCl); LiCl-wash buffer (0.25 M LiCl, 1 %
658 Nonidet P-40, 1 % Na-deoxycholate, 1 mM EDTA, 10 mM Tris-HCl) and TE-
659 wash buffer. Chromatin was eluted and decrosslinked from the beads by
660 incubation in 120 µl SDS containing elution-buffer (50 mM Tris-HCl pH 8.0, 10

mM EDTA, 1 % SDS) containing 200 mM NaCl at 65 °C overnight. Chromatin containing supernatant was separated from the beads by a magnetic rack. DNA was purified using a DNA Clean & Concentrator kit (Zymo Research). For ChIP-seq, 1–2 ng of ChIP DNA was used for library preparation, using the NEBNext Ultra II DNA Library prep Kit (E7370; NEB). Libraries were sequenced using an Illumina NextSeq 2000 sequencer 75 bp Single End.

Assay for Transposase-Accessible Chromatin using sequencing (ATAC-seq)

ATACseq was performed using the Omni-ATAC-seq protocol [73]. Briefly, 1x10^5 cells were treated with DNase I (200 U/ml, Worthington) at 37°C for 30 min, washed with cold PBS twice and resuspended in 1 ml cold RSB buffer (10 mM Tris-HCl pH 7.4, 10 mM NaCl, 3 mM MgCl2). Cells were pelleted again at 500 x g for 5 min and resuspended in 50 µl of cold ATAC-NTD lysis buffer (RSB Buffer + 0.1% NP40, 0.1% Tween-20, 0.01% Digitonin). Lysed cells were diluted in 1 ml cold ATAC-T buffer (RSB + 0.1% Tween-20) and inverted three times. The resulting nuclei were pelleted at 500 x g for 10 minutes and the supernatant was removed. Cell pellets were transposed with 50 µl of transposition mix containing 25 µl 2xTD Buffer (20 mM 1M Tris-HCl pH 7.6, 10 mM MgCl2, 20% Dimethyl Formamide), 2.5 µl transposase (custom made, 100nM final), 16.5 µl PBS, 0.5 µl 1% digitonin, 0.5 µl 10% Tween-20 and 5 µl H_2O) at 37°C and 1000 rpm on a thermomixer for 30 min. The reaction was

683 stopped by adding 250 µl of DNA Binding Buffer and DNA was isolated using
684 the Clean and Concentrator-5 Kit (Zymo). Libraries were produced by PCR
685 amplification of tagmented DNA and sequenced on a NextSeq 2000 sequencer
686 150 bp Paired End.
687
688 **Sequencing data processing**
689 For ChIPseq, quality filtered single end reads were aligned to the viral reference
690 genome of VZV (NC_001348.1) and human (hg38) using Bowtie [74] with
691 standard settings. Analysis of histone modification enrichment on the VZV
692 genome was done as described in [75].
693 For ATACseq, reads were processed using the PEPATAC pipeline [76]. Exact
694 integration sites were extended +/-25bp and visualized using IGV tools.
695 Average read density of ChIPseq and ATACseq data at human transcriptional
696 start sites (+/- 2.5kbp) was calculated and visualized using EaSeq [77].
697
698 **RNA in situ hybridization (RNAscope)**
699 RNAscope was performed using the RNAscope® Fluorescent Multiplex Kit
700 (ACD BioTechne). In brief, cells on 8-well chambers were fixed with 4% PFA
701 for 20 min at RT and overnight at 4 °C. On the next day, the cells were incubated
702 with RNAscope® hydrogen peroxide for 10 min at RT followed by protease
703 digestion for 10 min at RT. After washing with PBS, the cells were incubated
704 with pre-mixed target probe (RNAscope® Probe-V-VZV-O2, targeting VZV

VLT) or control probe (RNAscope® 3-Plex Negative control Probe/ RNAscope® 3-Plex Positive control Probe_Hs), both designed by ACD BioTechne, for 2 hours at 40°C in the HybEZ hybridization oven (ACD). Cells were washed with 1x wash buffer and incubated with amplification reagents (Amp 1 for 30 min, Amp 2 for 30 min and Amp 3 for 15 min at 40°C). After washing with 1x wash buffer, the cells were incubated with HRP adaptor for 15 min at 40°C, followed by incubation with the corresponding dye for 30 min at 40°C and incubated with HRP blocker for 15 min at 40°C. Cells were counterstained with DAPI and mounted onto glass slides with Prolong Gold Antifade Mountant (Thermo Fisher). Images were obtained using a Zeiss observer Z1 inverted microscope and Leica Inverted-3 microscope and analyzed by Fiji.

DNA in situ hybridization (DNAscope)

Viral DNA detection was performed using the RNAscope® Fluorescent Multiplex Kit (ACD BioTechne) with modifications using the RNAscope® Probe-V-VZV-O2, targeting VZV VLT, designed by ACD BioTechne. Briefly, we performed an RNase treatment with Resuspension buffer A1 containing RNase and 0.05% Tween-20 for 30 min at 40°C after the protease digestion step. The negative control wells were incubated with DNaseI for 40 min at 40°C after RNase treatment and washed 3 times with PBS containing 1 mM EDTA to inactivate DNaseI. We also performed a short denaturation step by incubating the 8-well chamber at 60°C with pre-warmed (60°C) probe for 10 min, and then

727 immediately transferred the chamber to the oven at 40°C, followed by
728 hybridization overnight. Amplification and detection were performed as
729 described for RNAscope (see above), using 0.5x wash buffer for all washing
730 steps.
731
732 **RNA-Seq library preparation and sequencing**
733 For each sample, polyadenylated (poly(A)) RNA was isolated from one
734 microgram of total RNA using the NEBNext Poly(A) mRNA Magnetic Isolation
735 Module. Reverse transcription, second strand synthesis, end-repair and A-
736 tailing were subsequently performed using the NEBNext Ultra II Directional
737 RNA Library prep kit. For the adaptor ligation step, we used TWIST Universal
738 Adapters from the standard TWIST Library Preparation Kit and omitted the
739 addition of NEB USER enzyme. Resulting libraries were subsequently amplified
740 (six cycles of PCR) using TWIST UDI primers and the Equinox Library Amp
741 Mix, all according to the protocols laid out in the TWIST Library Preparation
742 manual. Resulting libraries were purified using AMPure XP beads and
743 subsequently multiplexed in equimolar ratios. Hybridization was performed for
744 18 hours using biotinylated oligos designed by TWIST Biosciences against all
745 known VZV genome sequences. Post-hybridization washes and amplification
746 (18 cycles of PCR) were used to produce the final multiplexed library which was
747 subsequently sequenced on an Illumina MiSeq using a 2x150bp Micro Kit.
748

RNA-Seq analysis

Sequence data were de-multiplexed and individual sequence data sets were trimmed using the TrimGalore software (http://www.bioinformatics.babraham.ac.uk/projects/trim_galore/) to remove adaptor sequences and low-quality 3' ends. Sequence reads were competitively aligned against the human (HG38) and VZV genomes (strain Dumas, NC_001348) using STAR v2.7.9 (https://www.ncbi.nlm.nih.gov/pmc/articles/PMC3530905/). De-duplication of aligned reads was performed using picardtools MarkDuplicates (http://broadinstitute.github.io/picard). Resulting assemblies were parsed using SAMTools v1.15 (https://pubmed.ncbi.nlm.nih.gov/19505943/) and BEDTools v2.27 (https://pubmed.ncbi.nlm.nih.gov/20110278/) to produce bedgraphs that were visualized in Rstudio using the package GVIZ (https://pubmed.ncbi.nlm.nih.gov/27008022/).

Data availability

The RNAseq datasets generated and analysed in the current study are available in the European Nucleotide Archive (ENA) repository, with the following accession number: PRJEB68225. The ChIP-Seq and ATAC-Seq data for this study have been deposited in the ENA at EMBL-EBI under accession number PRJEB75685.

Acknowledgements

This work was funded by the Deutsche Forschungsgemeinschaft (DFG, German Research Foundation) under Germany's Excellence Strategy – EXC 2155 "RESIST" – project number 390874280 (https://www.resist-cluster.de/en/) and by the Deutsche Forschungsgemeinschaft (DFG, German Research Foundation) in the framework of the Research Unit FOR5200 DEEP-DV (443644894) projects VI 762/4-1 and KA 3492/12-1. J.W. and G.S. were funded by a fellowship from the China Scholarship Council No. 201908370216 and 201808230268, respectively. We thank Werner Ouwendijk and Georges Verjans (Erasmus MC, Rotterdam, The Netherlands) for providing the original protocol to produce cell-free VZV. We thank Jens Bohne (Institute of Virology, Hannover Medical School, Germany) for providing the lentivirus expressing eGFP. The funders had no role in study design, data collection and analysis, the decision to publish, or preparation of the manuscript.

References

1. Yawn BP, Saddier P, Wollan PC, St Sauver JL, Kurland MJ, Sy LS. A population-based study of the incidence and complication rates of herpes zoster before zoster vaccine introduction. Mayo Clin Proc. 2007;82(11):1341-9. doi: 10.4065/82.11.1341. PubMed PMID: 17976353.

2. Dworkin RH, Gnann JW, Jr., Oaklander AL, Raja SN, Schmader KE, Whitley RJ. Diagnosis and assessment of pain associated with herpes zoster and postherpetic neuralgia. J Pain. 2008;9(1 Suppl 1):S37-44. doi: 10.1016/j.jpain.2007.10.008. PubMed PMID: 18166464.

3. Zin CS, Nissen LM, Smith MT, O'Callaghan JP, Moore BJ. An update on the pharmacological management of post-herpetic neuralgia and painful diabetic neuropathy. CNS Drugs. 2008;22(5):417-42. doi: 10.2165/00023210-200822050-00005. PubMed PMID: 18399710.

4. Zerboni L, Sen N, Oliver SL, Arvin AM. Molecular mechanisms of varicella zoster virus pathogenesis. Nat Rev Microbiol. 2014;12(3):197-210. doi: 10.1038/nrmicro3215. PubMed PMID: 24509782; PubMed Central PMCID: PMCPMC4066823.

5. Gershon AA, Breuer J, Cohen JI, Cohrs RJ, Gershon MD, Gilden D, et al. Varicella zoster virus infection. Nat Rev Dis Primers. 2015;1:15016. doi: 10.1038/nrdp.2015.16. PubMed PMID: 27188665; PubMed Central PMCID: PMCPMC5381807.

808 6. Clarke P, Beer T, Cohrs R, Gilden DH. Configuration of latent varicella-zoster
809 virus DNA. J Virol. 1995;69(12):8151-4. Epub 1995/12/01. doi:
810 10.1128/jvi.69.12.8151-8154.1995. PubMed PMID: 7494340; PubMed Central
811 PMCID: PMCPMC189772.
812 7. Kennedy PG, Grinfeld E, Gow JW. Latent varicella-zoster virus is located
813 predominantly in neurons in human trigeminal ganglia. Proc Natl Acad Sci U S A.
814 1998;95(8):4658-62. Epub 1998/05/16. doi: 10.1073/pnas.95.8.4658. PubMed
815 PMID: 9539794; PubMed Central PMCID: PMCPMC22546.
816 8. Levin MJ, Cai GY, Manchak MD, Pizer LI. Varicella-zoster virus DNA in cells
817 isolated from human trigeminal ganglia. J Virol. 2003;77(12):6979-87. Epub
818 2003/05/28. doi: 10.1128/jvi.77.12.6979-6987.2003. PubMed PMID: 12768016;
819 PubMed Central PMCID: PMCPMC156183.
820 9. Wang K, Lau TY, Morales M, Mont EK, Straus SE. Laser-capture
821 microdissection: refining estimates of the quantity and distribution of latent
822 herpes simplex virus 1 and varicella-zoster virus DNA in human trigeminal Ganglia
823 at the single-cell level. J Virol. 2005;79(22):14079-87. Epub 2005/10/29. doi:
824 10.1128/jvi.79.22.14079-14087.2005. PubMed PMID: 16254342; PubMed Central
825 PMCID: PMCPMC1280223.
826 10. Gershon AA, Chen J, Gershon MD. Use of Saliva to Identify Varicella Zoster
827 Virus Infection of the Gut. Clin Infect Dis. 2015;61(4):536-44. Epub 2015/04/18.
828 doi: 10.1093/cid/civ320. PubMed PMID: 25882301; PubMed Central PMCID:
829 PMCPMC4607733.

830 11. Gershon M, Gershon A. Varicella-Zoster Virus and the Enteric Nervous
831 System. J Infect Dis. 2018;218(suppl_2):S113-s9. Epub 2018/09/25. doi:
832 10.1093/infdis/jiy407. PubMed PMID: 30247599; PubMed Central PMCID:
833 PMCPMC6151087.
834 12. Depledge DP, Sadaoka T, Ouwendijk WJD. Molecular Aspects of Varicella-
835 Zoster Virus Latency. Viruses. 2018;10(7). Epub 2018/07/01. doi:
836 10.3390/v10070349. PubMed PMID: 29958408; PubMed Central PMCID:
837 PMCPMC6070824.
838 13. Depledge DP, Ouwendijk WJD, Sadaoka T, Braspenning SE, Mori Y, Cohrs RJ,
839 et al. A spliced latency-associated VZV transcript maps antisense to the viral
840 transactivator gene 61. Nat Commun. 2018;9(1):1167. Epub 20180321. doi:
841 10.1038/s41467-018-03569-2. PubMed PMID: 29563516; PubMed Central
842 PMCID: PMCPMC5862956.
843 14. Ouwendijk WJD, Depledge DP, Rajbhandari L, Lenac Rovis T, Jonjic S, Breuer
844 J, et al. Varicella-zoster virus VLT-ORF63 fusion transcript induces broad viral gene
845 expression during reactivation from neuronal latency. Nat Commun.
846 2020;11(1):6324. doi: 10.1038/s41467-020-20031-4. PubMed PMID: 33303747;
847 PubMed Central PMCID: PMCPMC7730162.
848 15. Gowrishankar K, Slobedman B, Cunningham AL, Miranda-Saksena M, Boadle
849 RA, Abendroth A. Productive varicella-zoster virus infection of cultured intact
850 human ganglia. J Virol. 2007;81(12):6752-6. doi: 10.1128/JVI.02793-06. PubMed
851 PMID: 17409155; PubMed Central PMCID: PMCPMC1900131.

852 16. Hood C, Cunningham AL, Slobedman B, Boadle RA, Abendroth A. Varicella-
853 zoster virus-infected human sensory neurons are resistant to apoptosis, yet
854 human foreskin fibroblasts are susceptible: evidence for a cell-type-specific
855 apoptotic response. J Virol. 2003;77(23):12852-64. doi: 10.1128/jvi.77.23.12852-
856 12864.2003. PubMed PMID: 14610206; PubMed Central PMCID: PMCPMC262578.
857 17. Baird NL, Zhu S, Pearce CM, Viejo-Borbolla A. Current In Vitro Models to
858 Study Varicella Zoster Virus Latency and Reactivation. Viruses. 2019;11(2). doi:
859 10.3390/v11020103. PubMed PMID: 30691086; PubMed Central PMCID:
860 PMCPMC6409813.
861 18. Markus A, Lebenthal-Loinger I, Yang IH, Kinchington PR, Goldstein RS. An in
862 vitro model of latency and reactivation of varicella zoster virus in human stem cell-
863 derived neurons. PLoS Pathog. 2015;11(6):e1004885. doi:
864 10.1371/journal.ppat.1004885. PubMed PMID: 26042814; PubMed Central
865 PMCID: PMCPMC4456082.
866 19. Wilcox CL, Johnson EM, Jr. Nerve growth factor deprivation results in the
867 reactivation of latent herpes simplex virus in vitro. J Virol. 1987;61(7):2311-5. doi:
868 10.1128/JVI.61.7.2311-2315.1987. PubMed PMID: 3035230; PubMed Central
869 PMCID: PMCPMC283698.
870 20. Wilcox CL, Johnson EM, Jr. Characterization of nerve growth factor-
871 dependent herpes simplex virus latency in neurons in vitro. J Virol. 1988;62(2):393-
872 9. doi: 10.1128/JVI.62.2.393-399.1988. PubMed PMID: 2826804; PubMed Central
873 PMCID: PMCPMC250548.

874 21. Camarena V, Kobayashi M, Kim JY, Roehm P, Perez R, Gardner J, et al. Nature
875 and duration of growth factor signaling through receptor tyrosine kinases
876 regulates HSV-1 latency in neurons. Cell Host Microbe. 2010;8(4):320-30. doi:
877 10.1016/j.chom.2010.09.007. PubMed PMID: 20951966; PubMed Central PMCID:
878 PMCPMC2988476.
879 22. Kim JY, Mandarino A, Chao MV, Mohr I, Wilson AC. Transient reversal of
880 episome silencing precedes VP16-dependent transcription during reactivation of
881 latent HSV-1 in neurons. PLoS Pathog. 2012;8(2):e1002540. doi:
882 10.1371/journal.ppat.1002540. PubMed PMID: 22383875; PubMed Central
883 PMCID: PMCPMC3285597.
884 23. Cuddy SR, Schinlever AR, Dochnal S, Seegren PV, Suzich J, Kundu P, et al.
885 Neuronal hyperexcitability is a DLK-dependent trigger of herpes simplex virus
886 reactivation that can be induced by IL-1. Elife. 2020;9. doi: 10.7554/eLife.58037.
887 PubMed PMID: 33350386; PubMed Central PMCID: PMCPMC7773336.
888 24. Barrozo ER, Nakayama S, Singh P, Neumann DM, Bloom DC. Herpes Simplex
889 Virus 1 MicroRNA miR-H8 Is Dispensable for Latency and Reactivation In Vivo. J
890 Virol. 2021;95(4). doi: 10.1128/JVI.02179-20. PubMed PMID: 33208453; PubMed
891 Central PMCID: PMCPMC7851547.
892 25. Edwards TG, Bloom DC. Lund Human Mesencephalic (LUHMES) Neuronal Cell
893 Line Supports Herpes Simplex Virus 1 Latency In Vitro. J Virol. 2019;93(6). doi:
894 10.1128/JVI.02210-18. PubMed PMID: 30602607; PubMed Central PMCID:
895 PMCPMC6401467.

896 26. Sadaoka T, Depledge DP, Rajbhandari L, Venkatesan A, Breuer J, Cohen JI. In
897 vitro system using human neurons demonstrates that varicella-zoster vaccine
898 virus is impaired for reactivation, but not latency. Proc Natl Acad Sci U S A.
899 2016;113(17):E2403-12. doi: 10.1073/pnas.1522575113. PubMed PMID:
900 27078099; PubMed Central PMCID: PMCPMC4855584.
901 27. Pourchet A, Modrek AS, Placantonakis DG, Mohr I, Wilson AC. Modeling HSV-
902 1 Latency in Human Embryonic Stem Cell-Derived Neurons. Pathogens. 2017;6(2).
903 Epub 2017/06/09. doi: 10.3390/pathogens6020024. PubMed PMID: 28594343;
904 PubMed Central PMCID: PMCPMC5488658.
905 28. Markus A, Grigoryan S, Sloutskin A, Yee MB, Zhu H, Yang IH, et al. Varicella-
906 zoster virus (VZV) infection of neurons derived from human embryonic stem cells:
907 direct demonstration of axonal infection, transport of VZV, and productive
908 neuronal infection. J Virol. 2011;85(13):6220-33. Epub 2011/04/29. doi:
909 10.1128/jvi.02396-10. PubMed PMID: 21525353; PubMed Central PMCID:
910 PMCPMC3126485.
911 29. Zhu S, Stanslowsky N, Fernandez-Trillo J, Mamo TM, Yu P, Kalmbach N, et al.
912 Generation of hiPSC-derived low threshold mechanoreceptors containing axonal
913 termini resembling bulbous sensory nerve endings and expressing Piezo1 and
914 Piezo2. Stem Cell Res. 2021;56:102535. Epub 20210911. doi:
915 10.1016/j.scr.2021.102535. PubMed PMID: 34607262.
916 30. Zhu S, Stanslowsky N, Fernández-Trillo J, Mamo TM, Yu P, Kalmbach N, et al.
917 Generation of hiPSC-derived low threshold mechanoreceptors containing axonal

termini resembling bulbous sensory nerve endings and expressing Piezo1 and Piezo2. Stem Cell Res. 2021;56:102535. Epub 2021/10/05. doi: 10.1016/j.scr.2021.102535. PubMed PMID: 34607262.

31. Hu BY, Weick JP, Yu J, Ma LX, Zhang XQ, Thomson JA, et al. Neural differentiation of human induced pluripotent stem cells follows developmental principles but with variable potency. Proc Natl Acad Sci U S A. 2010;107(9):4335-40. Epub 2010/02/18. doi: 10.1073/pnas.0910012107. PubMed PMID: 20160098; PubMed Central PMCID: PMCPMC2840097 board member of Cellular Dynamics International (CDI). He also serves as a scientific advisor to and has financial interests in Tactics II Stem Cell Ventures.

32. Biedler JL, Helson L, Spengler BA. Morphology and growth, tumorigenicity, and cytogenetics of human neuroblastoma cells in continuous culture. Cancer Res. 1973;33(11):2643-52. PubMed PMID: 4748425.

33. Xicoy H, Wieringa B, Martens GJ. The SH-SY5Y cell line in Parkinson's disease research: a systematic review. Mol Neurodegener. 2017;12(1):10. doi: 10.1186/s13024-017-0149-0. PubMed PMID: 28118852; PubMed Central PMCID: PMCPMC5259880.

34. D'Aloia A, Pastori V, Blasa S, Campioni G, Peri F, Sacco E, et al. A new advanced cellular model of functional cholinergic-like neurons developed by reprogramming the human SH-SY5Y neuroblastoma cell line. Cell Death Discov. 2024;10(1):24. Epub 20240112. doi: 10.1038/s41420-023-01790-7. PubMed PMID: 38216593; PubMed Central PMCID: PMCPMC10786877.

940 35. Bell M, Zempel H. SH-SY5Y-derived neurons: a human neuronal model
941 system for investigating TAU sorting and neuronal subtype-specific TAU
942 vulnerability. Rev Neurosci. 2022;33(1):1-15. Epub 20210419. doi:
943 10.1515/revneuro-2020-0152. PubMed PMID: 33866701.
944 36. Christensen J, Steain M, Slobedman B, Abendroth A. Differentiated
945 neuroblastoma cells provide a highly efficient model for studies of productive
946 varicella-zoster virus infection of neuronal cells. J Virol. 2011;85(16):8436-42. doi:
947 10.1128/JVI.00515-11. PubMed PMID: 21632750; PubMed Central PMCID:
948 PMCPMC3147949.
949 37. Gerada C, Steain M, McSharry BP, Slobedman B, Abendroth A. Varicella-
950 Zoster Virus ORF63 Protects Human Neuronal and Keratinocyte Cell Lines from
951 Apoptosis and Changes Its Localization upon Apoptosis Induction. J Virol.
952 2018;92(12). doi: 10.1128/JVI.00338-18. PubMed PMID: 29593042; PubMed
953 Central PMCID: PMCPMC5974485.
954 38. Shipley MM, Mangold CA, Kuny CV, Szpara ML. Differentiated Human SH-
955 SY5Y Cells Provide a Reductionist Model of Herpes Simplex Virus 1 Neurotropism.
956 J Virol. 2017;91(23). doi: 10.1128/JVI.00958-17. PubMed PMID: 28956768;
957 PubMed Central PMCID: PMCPMC5686721.
958 39. Gimenez-Cassina A, Lim F, Diaz-Nido J. Differentiation of a human
959 neuroblastoma into neuron-like cells increases their susceptibility to transduction
960 by herpesviral vectors. J Neurosci Res. 2006;84(4):755-67. doi: 10.1002/jnr.20976.
961 PubMed PMID: 16802347.

962 40. Luo MH, Fortunato EA. Long-term infection and shedding of human
963 cytomegalovirus in T98G glioblastoma cells. J Virol. 2007;81(19):10424-36. doi:
964 10.1128/JVI.00866-07. PubMed PMID: 17652378; PubMed Central PMCID:
965 PMCPMC2045481.
966 41. Shipley MM, Mangold CA, Szpara ML. Differentiation of the SH-SY5Y Human
967 Neuroblastoma Cell Line. J Vis Exp. 2016;(108):53193. doi: 10.3791/53193.
968 PubMed PMID: 26967710; PubMed Central PMCID: PMCPMC4828168.
969 42. Tischer BK, Kaufer BB, Sommer M, Wussow F, Arvin AM, Osterrieder N. A self-
970 excisable infectious bacterial artificial chromosome clone of varicella-zoster virus
971 allows analysis of the essential tegument protein encoded by ORF9. J Virol.
972 2007;81(23):13200-8. Epub 20071003. doi: 10.1128/JVI.01148-07. PubMed PMID:
973 17913822; PubMed Central PMCID: PMCPMC2169085.
974 43. Braspenning SE, Sadaoka T, Breuer J, Verjans G, Ouwendijk WJD, Depledge
975 DP. Decoding the Architecture of the Varicella-Zoster Virus Transcriptome. mBio.
976 2020;11(5). Epub 20201006. doi: 10.1128/mBio.01568-20. PubMed PMID:
977 33024035; PubMed Central PMCID: PMCPMC7542360.
978 44. Jurgens C, Ssebyatika G, Beyer S, Pluckebaum N, Kropp KA, Gonzalez-Motos
979 V, et al. Viral modulation of type II interferon increases T cell adhesion and virus
980 spread. bioRxiv. 2023. Epub 20230526. doi: 10.1101/2023.05.26.542397. PubMed
981 PMID: 37292914; PubMed Central PMCID: PMCPMC10246016.
982 45. Bhatt S, Ashlock BM, Toomey NL, Diaz LA, Mesri EA, Lossos IS, et al. Efficacious
983 proteasome/HDAC inhibitor combination therapy for primary effusion lymphoma.

984 J Clin Invest. 2013;123(6):2616-28. Epub 2013/05/03. doi: 10.1172/jci64503.
985 PubMed PMID: 23635777; PubMed Central PMCID: PMCPMC3668825.
986 46. Cheung YT, Lau WK, Yu MS, Lai CS, Yeung SC, So KF, et al. Effects of all-trans-
987 retinoic acid on human SH-SY5Y neuroblastoma as in vitro model in neurotoxicity
988 research. Neurotoxicology. 2009;30(1):127-35. Epub 2008/12/06. doi:
989 10.1016/j.neuro.2008.11.001. PubMed PMID: 19056420.
990 47. Guarnieri S, Pilla R, Morabito C, Sacchetti S, Mancinelli R, Fanò G, et al.
991 Extracellular guanosine and GTP promote expression of differentiation markers
992 and induce S-phase cell-cycle arrest in human SH-SY5Y neuroblastoma cells. Int
993 J Dev Neurosci. 2009;27(2):135-47. Epub 2008/12/30. doi:
994 10.1016/j.ijdevneu.2008.11.007. PubMed PMID: 19111604.
995 48. Kovalevich J, Langford D. Considerations for the use of SH-SY5Y
996 neuroblastoma cells in neurobiology. Methods Mol Biol. 2013;1078:9-21. Epub
997 2013/08/27. doi: 10.1007/978-1-62703-640-5_2. PubMed PMID: 23975817;
998 PubMed Central PMCID: PMCPMC5127451.
999 49. La Monica N, Racaniello VR. Differences in replication of attenuated and
1000 neurovirulent polioviruses in human neuroblastoma cell line SH-SY5Y. J Virol.
1001 1989;63(5):2357-60. doi: 10.1128/JVI.63.5.2357-2360.1989. PubMed PMID:
1002 2539524; PubMed Central PMCID: PMCPMC250657.
1003 50. Sanchez-San Martin C, Li T, Bouquet J, Streithorst J, Yu G, Paranjpe A, et al.
1004 Differentiation enhances Zika virus infection of neuronal brain cells. Sci Rep.

2018;8(1):14543. doi: 10.1038/s41598-018-32400-7. PubMed PMID: 30266962; PubMed Central PMCID: PMCPMC6162312.

51. Christensen J, Steain M, Slobedman B, Abendroth A. Varicella-zoster virus glycoprotein I is essential for spread in dorsal root ganglia and facilitates axonal localization of structural virion components in neuronal cultures. J Virol. 2013;87(24):13719-28. Epub 2013/10/11. doi: 10.1128/jvi.02293-13. PubMed PMID: 24109230; PubMed Central PMCID: PMCPMC3838295.

52. Jiang HF, Wang W, Jiang X, Zeng WB, Shen ZZ, Song YG, et al. ORF7 of Varicella-Zoster Virus Is Required for Viral Cytoplasmic Envelopment in Differentiated Neuronal Cells. J Virol. 2017;91(12). Epub 20170526. doi: 10.1128/JVI.00127-17. PubMed PMID: 28356523; PubMed Central PMCID: PMCPMC5446663.

53. Cliffe AR, Garber DA, Knipe DM. Transcription of the herpes simplex virus latency-associated transcript promotes the formation of facultative heterochromatin on lytic promoters. J Virol. 2009;83(16):8182-90. Epub 2009/06/12. doi: 10.1128/jvi.00712-09. PubMed PMID: 19515781; PubMed Central PMCID: PMCPMC2715743.

54. Kwiatkowski DL, Thompson HW, Bloom DC. The polycomb group protein Bmi1 binds to the herpes simplex virus 1 latent genome and maintains repressive histone marks during latency. J Virol. 2009;83(16):8173-81. Epub 2009/06/12. doi: 10.1128/jvi.00686-09. PubMed PMID: 19515780; PubMed Central PMCID: PMCPMC2715759.

1027 55. Reichelt M, Wang L, Sommer M, Perrino J, Nour AM, Sen N, et al. Entrapment
1028 of viral capsids in nuclear PML cages is an intrinsic antiviral host defense against
1029 varicella-zoster virus. PLoS Pathog. 2011;7(2):e1001266. Epub 20110203. doi:
1030 10.1371/journal.ppat.1001266. PubMed PMID: 21304940; PubMed Central
1031 PMCID: PMCPMC3033373.
1032 56. Scherer M, Read C, Neusser G, Kranz C, Kuderna AK, Müller R, et al. Dual
1033 signaling via interferon and DNA damage response elicits entrapment by giant
1034 PML nuclear bodies. Elife. 2022;11. Epub 2022/03/24. doi: 10.7554/eLife.73006.
1035 PubMed PMID: 35319461; PubMed Central PMCID: PMCPMC8975554.
1036 57. Irwan ID, Cullen BR. The SMC5/6 complex: An emerging antiviral restriction
1037 factor that can silence episomal DNA. PLoS Pathog. 2023;19(3):e1011180. Epub
1038 20230302. doi: 10.1371/journal.ppat.1011180. PubMed PMID: 36862666; PubMed
1039 Central PMCID: PMCPMC9980727.
1040 58. Xu W, Ma C, Zhang Q, Zhao R, Hu D, Zhang X, et al. PJA1 Coordinates with
1041 the SMC5/6 Complex To Restrict DNA Viruses and Episomal Genes in an
1042 Interferon-Independent Manner. J Virol. 2018;92(22). Epub 20181029. doi:
1043 10.1128/JVI.00825-18. PubMed PMID: 30185588; PubMed Central PMCID:
1044 PMCPMC6206484.
1045 59. Sodroski CN, Knipe DM. Nuclear interferon-stimulated gene product
1046 maintains heterochromatin on the herpes simplex viral genome to limit lytic
1047 infection. Proc Natl Acad Sci U S A. 2023;120(45):e2310996120. Epub 2023/10/26.

1048 doi: 10.1073/pnas.2310996120. PubMed PMID: 37883416; PubMed Central
1049 PMCID: PMCPMC10636318.
1050 60. Orzalli MH, Conwell SE, Berrios C, DeCaprio JA, Knipe DM. Nuclear interferon-
1051 inducible protein 16 promotes silencing of herpesviral and transfected DNA. Proc
1052 Natl Acad Sci U S A. 2013;110(47):E4492-501. Epub 2013/11/08. doi:
1053 10.1073/pnas.1316194110. PubMed PMID: 24198334; PubMed Central PMCID:
1054 PMCPMC3839728.
1055 61. Merkl PE, Orzalli MH, Knipe DM. Mechanisms of Host IFI16, PML, and Daxx
1056 Protein Restriction of Herpes Simplex Virus 1 Replication. J Virol. 2018;92(10).
1057 Epub 2018/03/02. doi: 10.1128/jvi.00057-18. PubMed PMID: 29491153; PubMed
1058 Central PMCID: PMCPMC5923075.
1059 62. Merkl PE, Knipe DM. Role for a Filamentous Nuclear Assembly of IFI16, DNA,
1060 and Host Factors in Restriction of Herpesviral Infection. mBio. 2019;10(1). Epub
1061 20190122. doi: 10.1128/mBio.02621-18. PubMed PMID: 30670617; PubMed
1062 Central PMCID: PMCPMC6343039.
1063 63. Dressler GR, Rock DL, Fraser NW. Latent herpes simplex virus type 1 DNA is
1064 not extensively methylated in vivo. J Gen Virol. 1987;68 (Pt 6):1761-5. doi:
1065 10.1099/0022-1317-68-6-1761. PubMed PMID: 3035069.
1066 64. Kubat NJ, Tran RK, McAnany P, Bloom DC. Specific histone tail modification
1067 and not DNA methylation is a determinant of herpes simplex virus type 1 latent
1068 gene expression. J Virol. 2004;78(3):1139-49. doi: 10.1128/jvi.78.3.1139-
1069 1149.2004. PubMed PMID: 14722269; PubMed Central PMCID: PMCPMC321404.

1070 65. Goodwin TJ, McCarthy M, Cohrs RJ, Kaufer BB. 3D tissue-like assemblies: A
1071 novel approach to investigate virus-cell interactions. Methods. 2015;90:76-84.
1072 doi: 10.1016/j.ymeth.2015.05.010. PubMed PMID: 25986169.
1073 66. Goodwin TJ, McCarthy M, Osterrieder N, Cohrs RJ, Kaufer BB. Three-
1074 dimensional normal human neural progenitor tissue-like assemblies: a model of
1075 persistent varicella-zoster virus infection. PLoS pathogens. 2013;9(8):e1003512.
1076 Epub 2013/08/13. doi: 10.1371/journal.ppat.1003512. PubMed PMID: 23935496;
1077 PubMed Central PMCID: PMC3731237.
1078 67. Tischer BK, von Einem J, Kaufer B, Osterrieder N. Two-step red-mediated
1079 recombination for versatile high-efficiency markerless DNA manipulation in
1080 Escherichia coli. Biotechniques. 2006;40(2):191-7. PubMed PMID: 16526409.
1081 68. Tischer BK, Kaufer BB. Viral bacterial artificial chromosomes: generation,
1082 mutagenesis, and removal of mini-F sequences. Journal of biomedicine &
1083 biotechnology. 2012;2012:472537. Epub 2012/04/13. doi: 10.1155/2012/472537.
1084 PubMed PMID: 22496607; PubMed Central PMCID: PMC3303620.
1085 69. Kaufer BB, Smejkal B, Osterrieder N. The varicella-zoster virus ORFS/L (ORF0)
1086 gene is required for efficient viral replication and contains an element involved in
1087 DNA cleavage. J Virol. 2010;84(22):11661-9.
1088 70. Schambach A, Mueller D, Galla M, Verstegen MM, Wagemaker G, Loew R, et
1089 al. Overcoming promoter competition in packaging cells improves production of
1090 self-inactivating retroviral vectors. Gene Ther. 2006;13(21):1524-33. Epub
1091 20060608. doi: 10.1038/sj.gt.3302807. PubMed PMID: 16763662.

71. Ladner CL, Yang J, Turner RJ, Edwards RA. Visible fluorescent detection of proteins in polyacrylamide gels without staining. Anal Biochem. 2004;326(1):13-20. Epub 2004/02/11. doi: 10.1016/j.ab.2003.10.047. PubMed PMID: 14769330.

72. Gunther T, Grundhoff A. The epigenetic landscape of latent Kaposi sarcoma-associated herpesvirus genomes. PLoS Pathog. 2010;6(6):e1000935. Epub 20100603. doi: 10.1371/journal.ppat.1000935. PubMed PMID: 20532208; PubMed Central PMCID: PMCPMC2880564.

73. Corces MR, Trevino AE, Hamilton EG, Greenside PG, Sinnott-Armstrong NA, Vesuna S, et al. An improved ATAC-seq protocol reduces background and enables interrogation of frozen tissues. Nat Methods. 2017;14(10):959-62. Epub 20170828. doi: 10.1038/nmeth.4396. PubMed PMID: 28846090; PubMed Central PMCID: PMCPMC5623106.

74. Langmead B, Trapnell C, Pop M, Salzberg SL. Ultrafast and memory-efficient alignment of short DNA sequences to the human genome. Genome Biol. 2009;10(3):R25. Epub 20090304. doi: 10.1186/gb-2009-10-3-r25. PubMed PMID: 19261174; PubMed Central PMCID: PMCPMC2690996.

75. Gunther T, Frohlich J, Herrde C, Ohno S, Burkhardt L, Adler H, et al. A comparative epigenome analysis of gammaherpesviruses suggests cis-acting sequence features as critical mediators of rapid polycomb recruitment. PLoS Pathog. 2019;15(10):e1007838. Epub 20191031. doi: 10.1371/journal.ppat.1007838. PubMed PMID: 31671162; PubMed Central PMCID: PMCPMC6932816.

76. Smith JP, Corces MR, Xu J, Reuter VP, Chang HY, Sheffield NC. PEPATAC: an optimized pipeline for ATAC-seq data analysis with serial alignments. NAR Genom Bioinform. 2021;3(4):lqab101. Epub 20211123. doi: 10.1093/nargab/lqab101. PubMed PMID: 34859208; PubMed Central PMCID: PMCPMC8632735.

77. Lerdrup M, Johansen JV, Agrawal-Singh S, Hansen K. An interactive environment for agile analysis and visualization of ChIP-sequencing data. Nat Struct Mol Biol. 2016;23(4):349-57. Epub 20160229. doi: 10.1038/nsmb.3180. PubMed PMID: 26926434.

Figure legends:

Figure 1: Successful differentiation of SH-SY5Y into neuron-like cells. (**A**) Schematic representation of the differentiation process showing representative pictures of SH-SY5Y before treatment with collagenase (left) at day 10 post-differentiation, epithelial-like cells that remained in the well (middle) and neuron-like cells after seeding onto a new Matrigel-coated well. Scale bar: 100 µm. (**B**) Representative pictures of SH-SY5Y during the differentiation process. Scale bar: 100 µm. (**C**) Representative pictures showing expression of neuronal markers in dSH-SY5Y at 18 dpd. Scale bar: 10 µm. (**D**) Representative images showing KI67 expression in SH-SY5Y during the differentiation process. Scale bar: 20 µm. Abbreviations / acronyms: dpd, days post-differentiation; MAP2, microtubule-associated protein 2; DBH, dopamine beta-hydroxylase; Nav1.7, voltage-gated sodium channel Nav1.7; TuJ1, beta-III-tubulin antibody.

Figure 2: VZV productively infects dSH-SY5Y. (**A**) Schematic representation of the recombinant v63R/11G showing the terminal repeats long and short (TR_L and TR_S, respectively) the unique long and short regions (U_L and U_S, respectively) and the internal repeat short (IR_S). ORF63 and ORF70 correspond to duplications of the same ORF, with ORF63 located in the IR_S and ORF70 in the TR_S. (**B**) Images showing spread of v63R/11G in dSH-SY5Y cells. (**C-F**) Graphs showing VZV genome copies n=3-9 (B) and relative expression of VZV genes, n=3-6 (C-E) at different times post-infection. Abbreviations: dpi, days

post-infection. The results in (B-E) are from 3 biological replicates. Values are presented as mean ± s.e.m.

Figure 3: Incubation with ACV progressively represses VZV in dSH-SY5Y. (**A**) Schematic representation of the experiment. (**B**) Graph showing the day post-infection when wells containing ORF63-RFP/ORF11-GFP positive dSH-SY5Y cells were detected following incubation with ACV for 2-6 days. Each symbol represents one well containing ORF63-RFP/ORF11-GFP positive cells. “n” refers to the number of wells infected with VZV for each condition. (**C**) Graph showing the number of wells containing ORF63-RFP/ORF11-GFP positive (orange) and negative (blue) dSH-SY5Y cells following incubation with ACV for 2-6 days. The percentage on top of each column indicates the percentage of wells with ORF63-RFP/ORF11-GFP positive dSH-SY5Y cells at the end of the experiment (30 dpi). Abbreviations: dpi, days post-infection.

Figure 4: Incubation with ACV during 5 days results in a repressive phenotype that can be released. (**A**) Schematic representation of the experiment. (**B**) Representative images showing dSH-SY5Y cells infected with v63R/11G in the absence (acute) or presence of ACV for 5 dpi and lacking or containing ORF63-RFP/ORF11-GFP positive dSH-SY5Y cells. The dSH-SY5Y cells were labelled with an anti-TuJ1 antibody and the nuclei were stained with DAPI. Scale bar: 100 µm. (**C**) Western blot detecting VZV gE (top blot) and

actin (bottom blot) in dSH-SY5Y cell lysates obtained from mock- or v63R/11G-infected cells without ACV (acute) or with 5 days incubation with ACV. (**D-F**) Relative gene expression of VZV genes, n=3-9 (D,E) and quantification of VZV genomes, n=3-9 (F) in mock- or v63R/11G-infected dSH-SY5Y cells in the absence (acute) or presence of ACV for 5 dpi. (**G**) Detection of VZV genomes by *in situ* hybridization in dSH-SY5Y infected with v63R/11G in the presence of ACV for 5 days in wells where no ORF63-RFP/ORF11-GFP positive cells were detected. DAPI was used to stain nuclei. The white arrows point to the VZV genomes. Scale bar: 10 µm. (**H**) Detection of ORF63-RFP/ORF11-GFP in ARPE19 cells incubated with dSH-SY5Y cells (infected in the presence of ACV for 5 days) from wells lacking (NR) or containing (R) ORF63-RFP/ORF11-GFP-positive cells. DAPI was used to stain nuclei. In all panels NR refers to “non-replicating” VZV, while R refers to “replicating” VZV, determined by the expression of ORF63-RFP/ORF11-GFP. Abbreviations: dpi, days post-infection. The results in (D-F) are from 3 biological replicates. The images in (G) are representative from more than six samples. Values are presented as mean ± s.e.m.

Figure 5: A small percentage of dSH-SY5Y cells incubated with ACV for six days maintain non-replicating viral genomes for up to 20 days. (**A**) Schematic representation of the experiment. (**B**) Representative images showing dSH-SY5Y cells infected with v63R/11G in the absence (acute) or

presence of ACV for 6 dpi and lacking or containing ORF63-RFP/ORF11-GFP positive dSH-SY5Y cells. The dSH-SY5Y cells were labelled with an anti-TuJ1 antibody and the nuclei were stained with DAPI. Scale bar: 100 µm. (**C**) Western blot detecting VZV gE and IE4 (top blot) and actin (bottom blot) in dSH-SY5Y cell lysates obtained from mock- or v63R/11G-infected cells without ACV (acute) or with 6 days incubation with ACV. (**D-G**) Relative gene expression of VZV genes, n=3-6 (D-F) and quantification of VZV genomes, n=3-6 (G) in mock- or v63R/11G-infected dSH-SY5Y cells in the absence (acute) or presence of ACV for 6 dpi. (**H**) Detection of VZV genomes (grey dots) by *in situ* hybridization in dSH-SY5Y cells infected with v63R/11G in the absence (acute) and presence of ACV for 6 days in wells where no ORF63-RFP/ORF11-GFP positive cells were detected. DAPI was used to stain nuclei. The white arrow points to the VZV genome. Scale bar: 10 µm. Abbreviations: dpi, days post-infection. The results in (D-G) are from 3 biological replicates. Values are presented as mean ± s.e.m.

Figure 6: Incubation with ACV progressively represses VZV in dSH-SY5Y. (**A**) Schematic representation of the experiment. (**B**) Relative VZV gene expression in dSH-SY5Y cells infected with v63R/11G in the presence of ACV for 6 days and incubated with LY294002 or SAHA at 8 dpi, n=3-4. The results are from 3 biological replicates. Values are presented as mean ± s.e.m. (**C**) Representative images of dSH-SY5Y infected cells in the absence (acute) or

presence of ACV during 6 days and incubated or nor with LY294002 or SAHA at 8 dpi during 4 days. The pictures were taken at 6 dpi for acute infected cells and at 14 dpi for the samples treated with ACV. (**D**) Representative images of dSH-SY5Y cells infected with v63R/11G in the presence of ACV for 6 days and transduced with a lentivirus expressing VLT-ORF63 (top) or eGFP (bottom). The left and middle panels show direct fluorescent expression of ORF63-RFP, ORF11-GFP, RFP and GFP, while the right panels show the merge of the fluorescent channels with phase-contrast images. Scale bar: 100 µm. (**E**) Graphs showing the percentage and number of wells containing ORF63-RFP/ORF11-GFP positive dSH-SY5Y cells (representing replicating virus), following transduction with lentivirus expressing VLT-ORF63 or eGFP.

Figure 7: Incubation with ACV leads to low level genome-wide VZV transcription in dSH-SY5Y cells. (**A,B**) Genome-wide transcription profiles of dSH-SY5Y cells infected with v63R/11G in the absence (acute, violet) and presence of ACV for 6 dpi (orange, A; blue, B) or for 3, 4, 5 and 6 dpi (orange, B). Bulk RNA-Seq was performed at different times post-infection, as labelled. Transcription from both DNA strands is shown with the depth of coverage labelled on the y-axis. A representation of the VZV genome and all encoded transcripts is shown. (**C**) Detection by *in situ* hybridization of VZV mRNA (greydots) with a probe that detects VLT and VLT-ORF63 transcripts in dSH-SY5Y infected in the absence (acute) or presence of ACV for 6 days in wells

where no ORF63-RFP/ORF11-GFP positive cells were detected. DAPI was used to stain nuclei. The white arrow points to the transcript. Scale bar: 10 µm. Abbreviations: dpi, days post-infection.

Figure 8: ChIP-seq and ATAC-seq analysis of differentiated SH-SY5Y cells quiescently infected with VZV at 13 days post-infection. (**A**) Read density coverage tracks of histone marks and ATAC-seq signal on two host loci and VZV, determined by ChIP-seq. (**B**) Average read density of ChIP-seq and ATAC-seq reads at all human TSS (+/- 2.5kb). (**C**) Input-normalized quantification of ChIP-seq signals in a 10 kb sliding window across the VZV genome (VZV, right panel), relative to the 200 most significantly enriched host regions (hg38 positives, left panel) and an equal number of size matched, randomly selected host control loci (hg38 random, center). Signals observed in host control regions were set to 1 (10E0). Experiments were independently performed with VZV BAC pOka (WT) and v63R/11G. (**D**) Input-normalized quantification quantification of ATAC-seq coverage at all positive host sites (n=54760) compared to a count/size-matched collection of randomly selected control regions and 500bp sliding windows across the VZV genome (n=249).

Figure 1

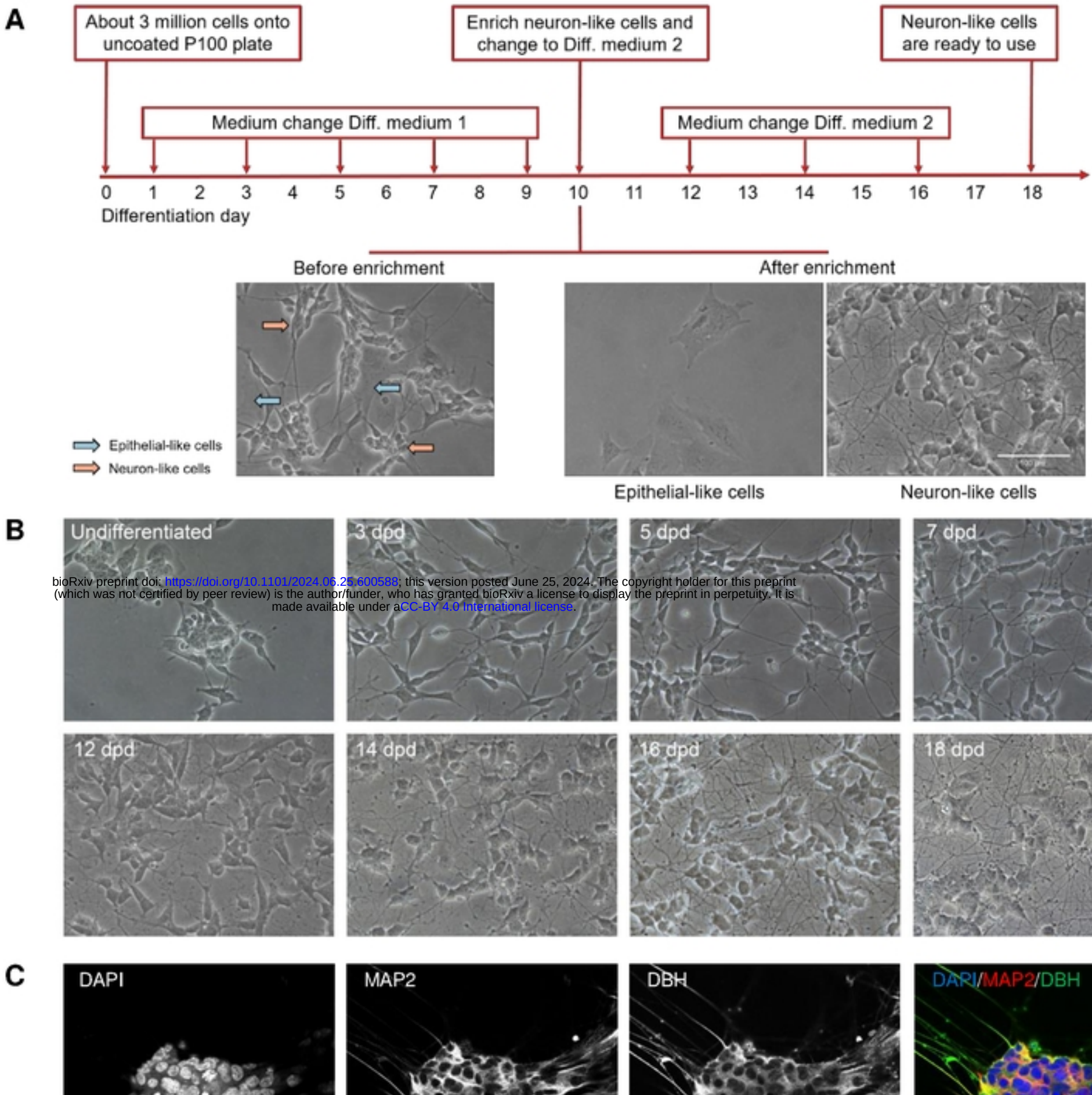

Figure 1

Figure 2

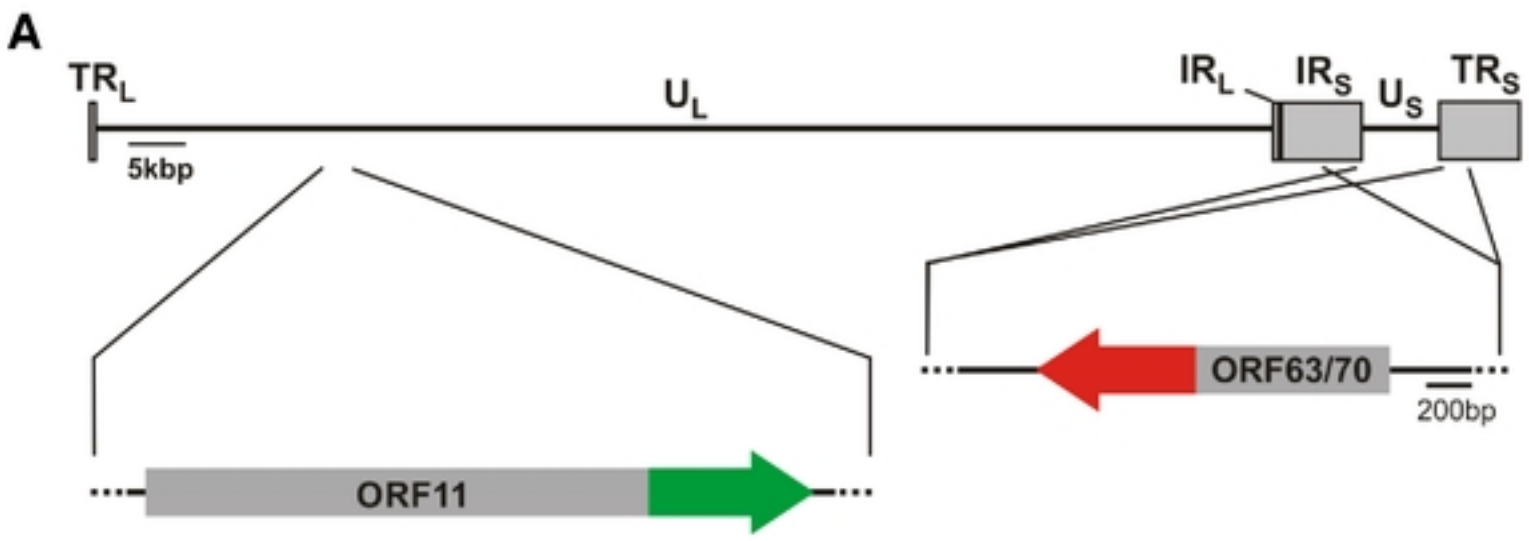

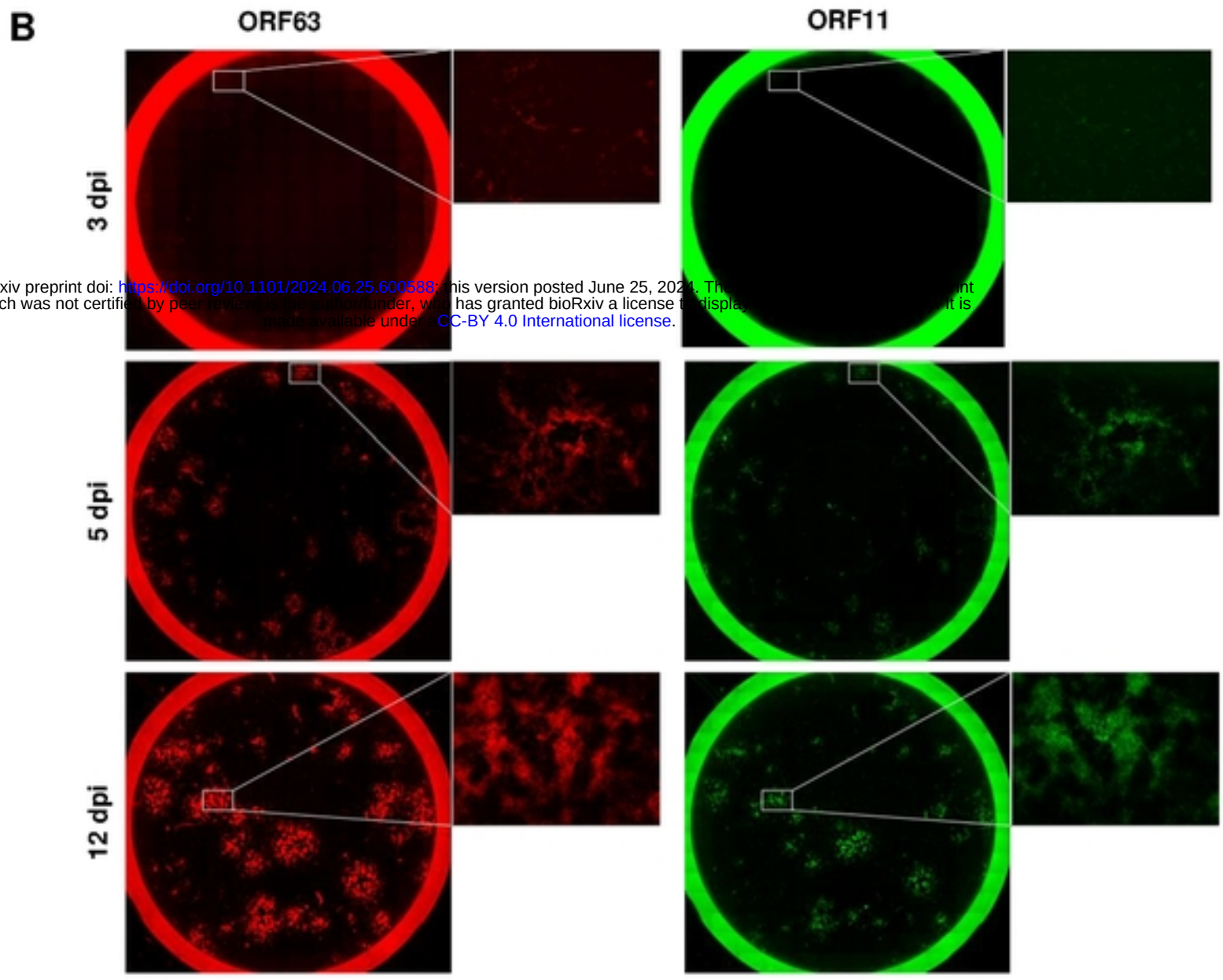

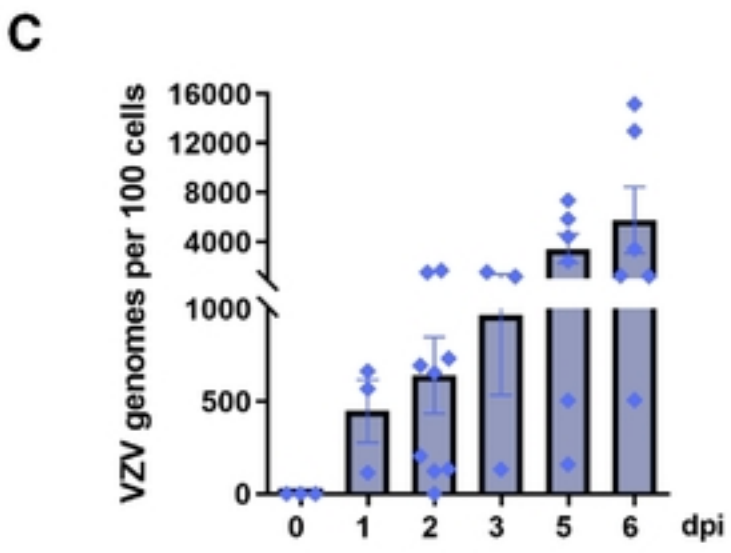

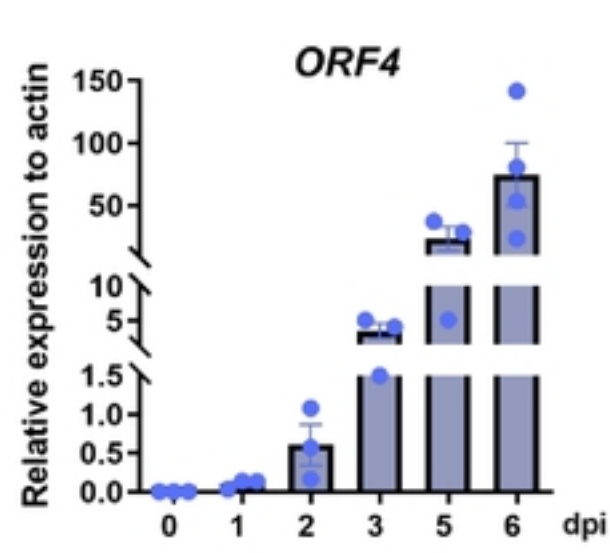

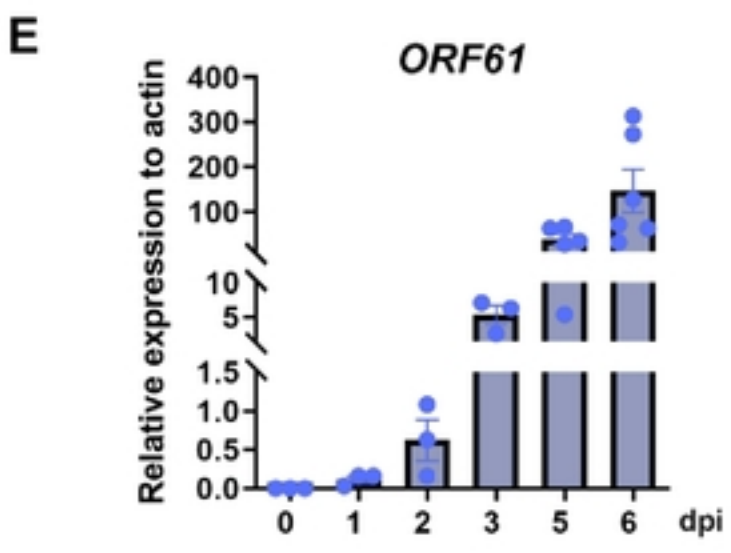

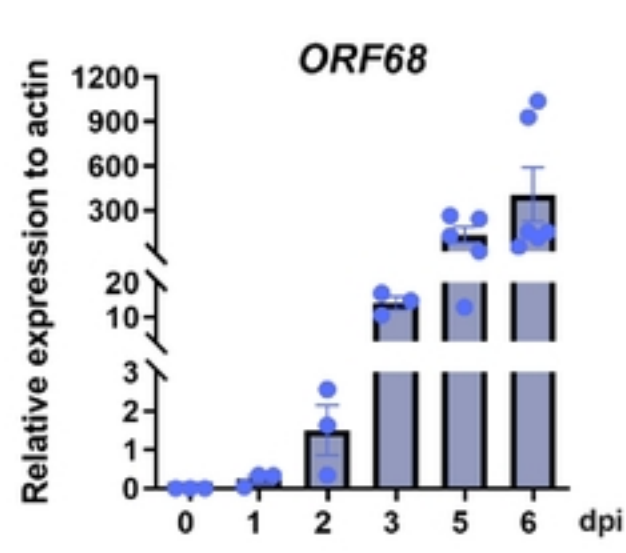

Figure 3

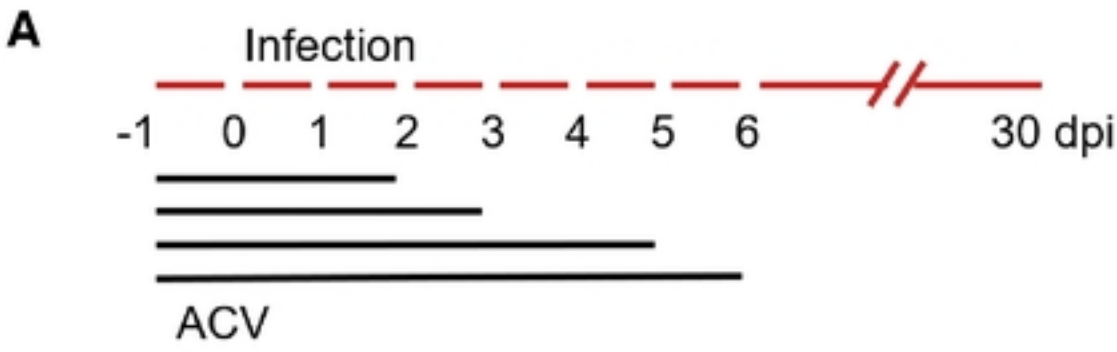

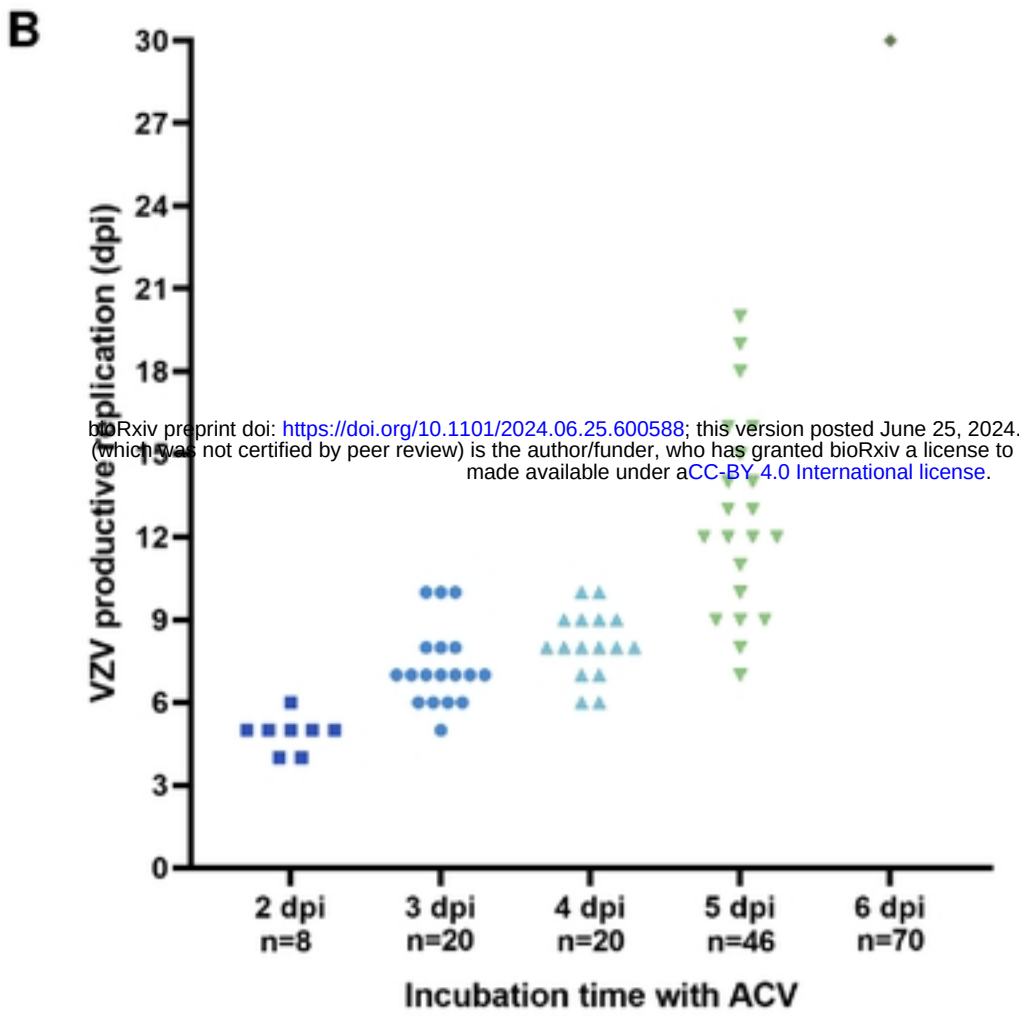

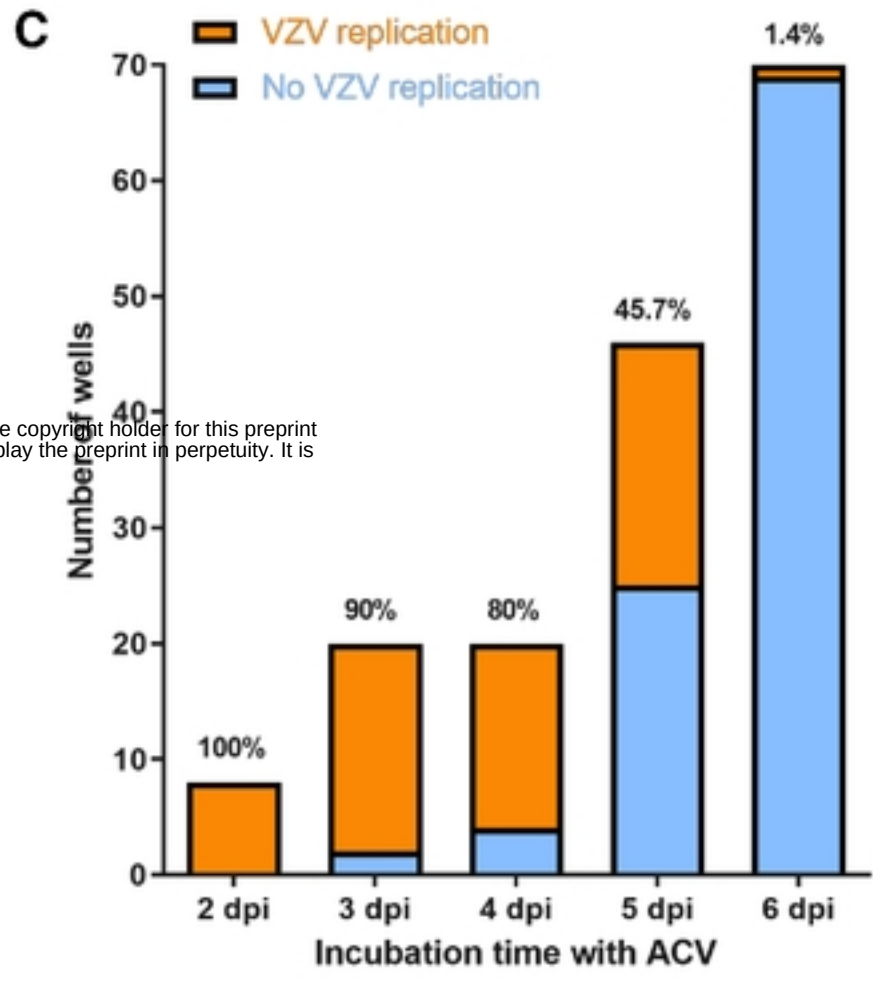

Figure 3

Figure 4

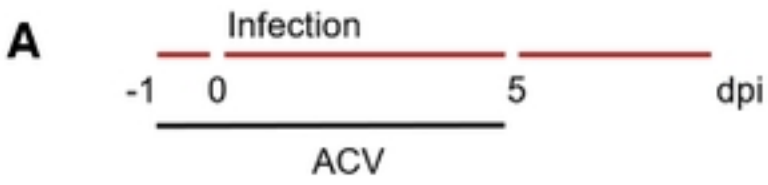

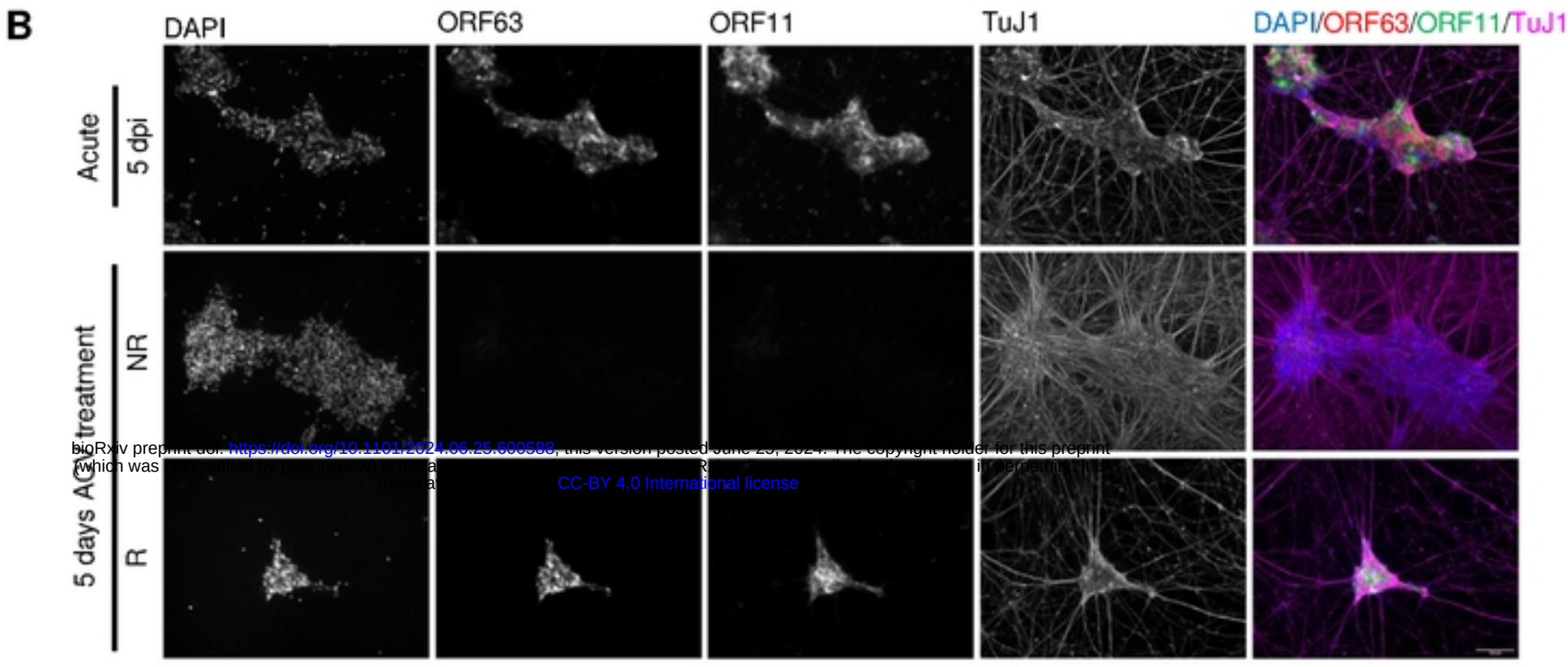

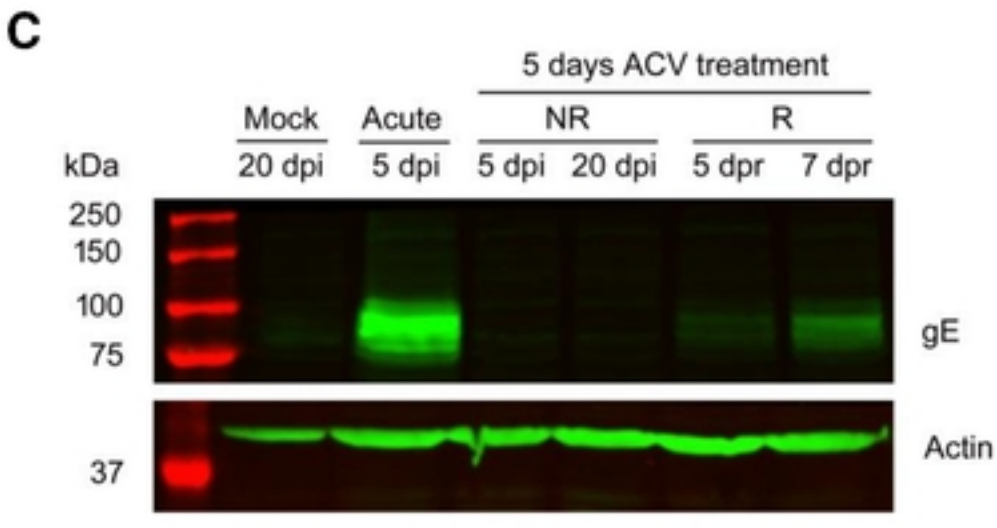

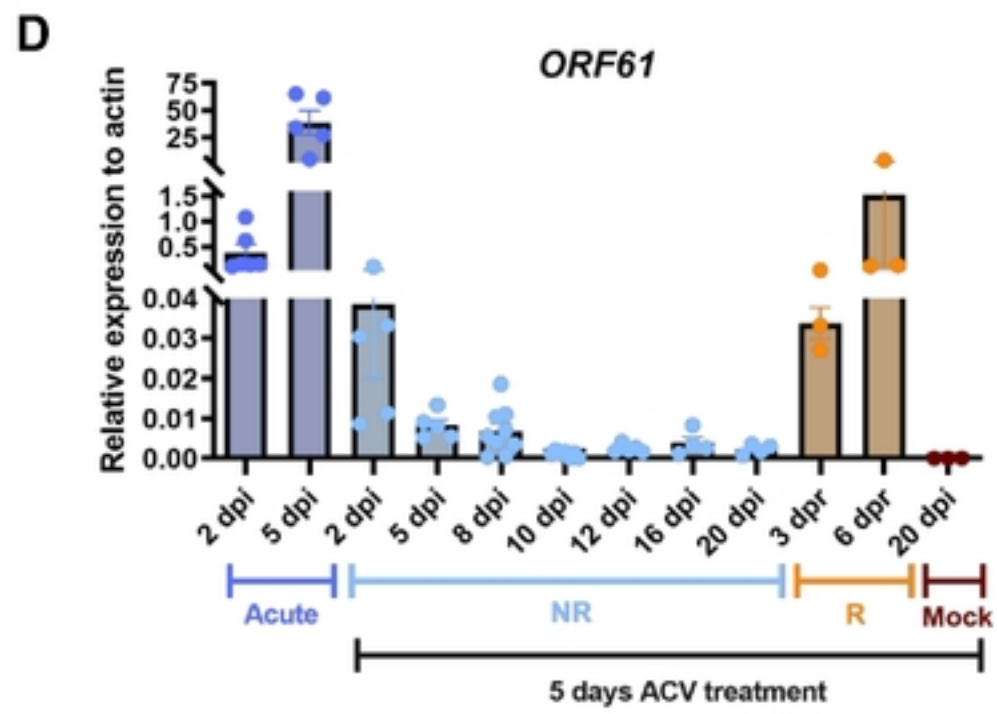

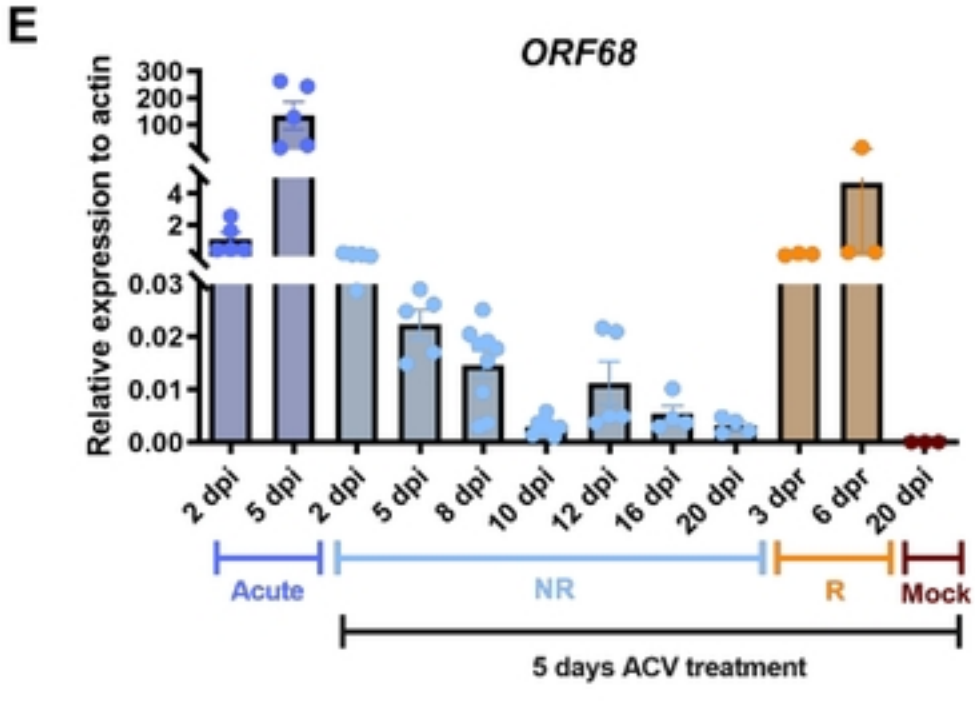

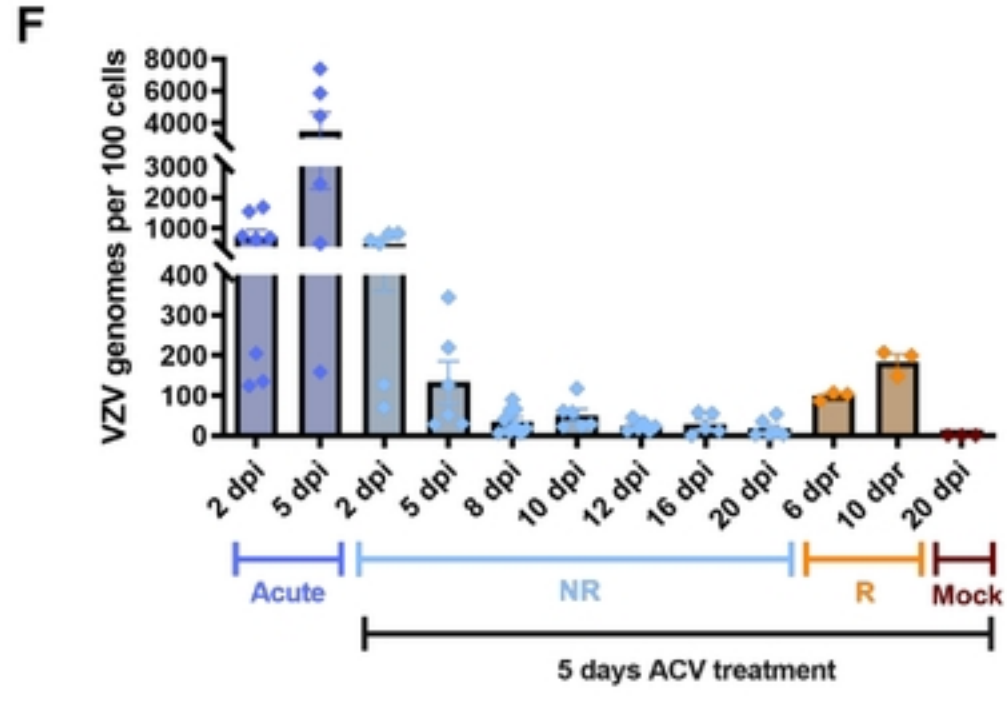

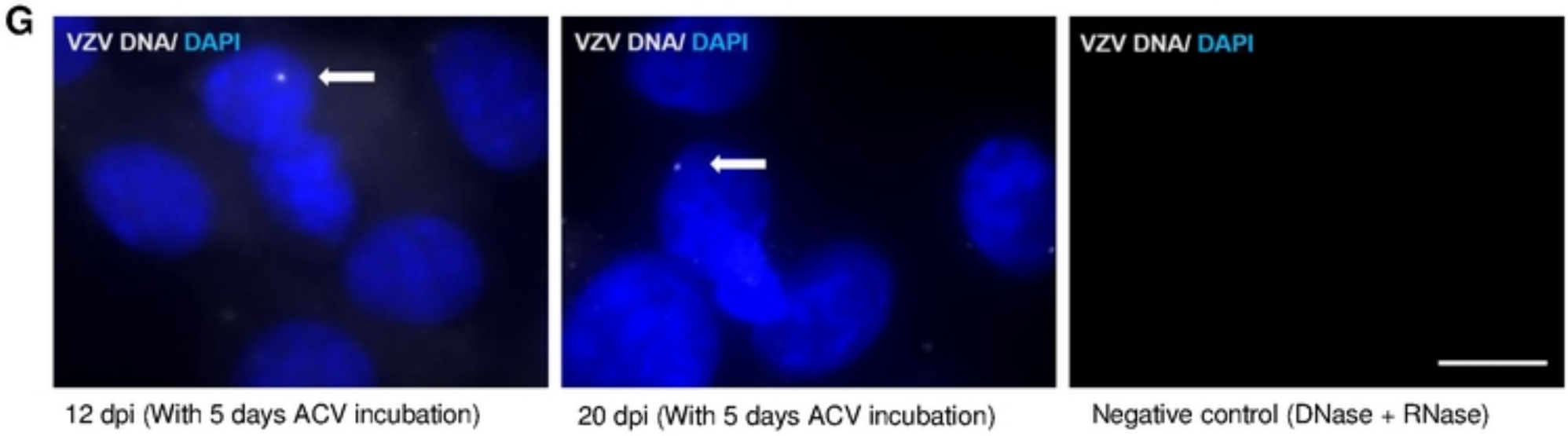

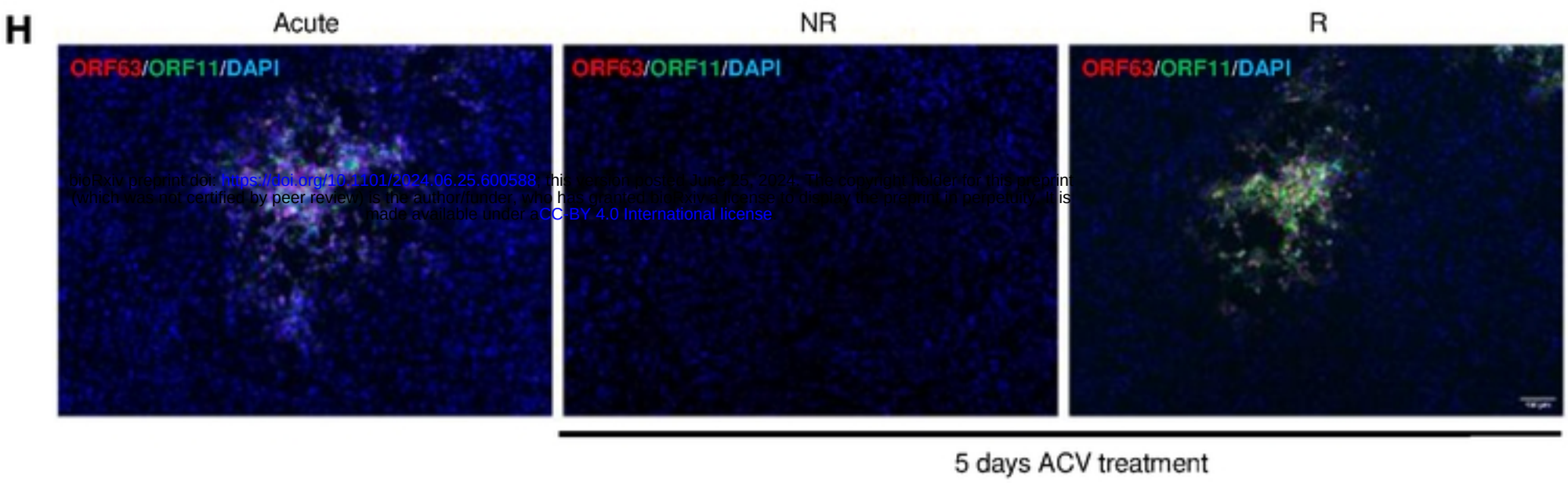

Figure 5

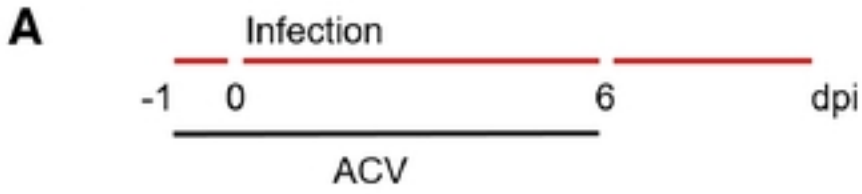

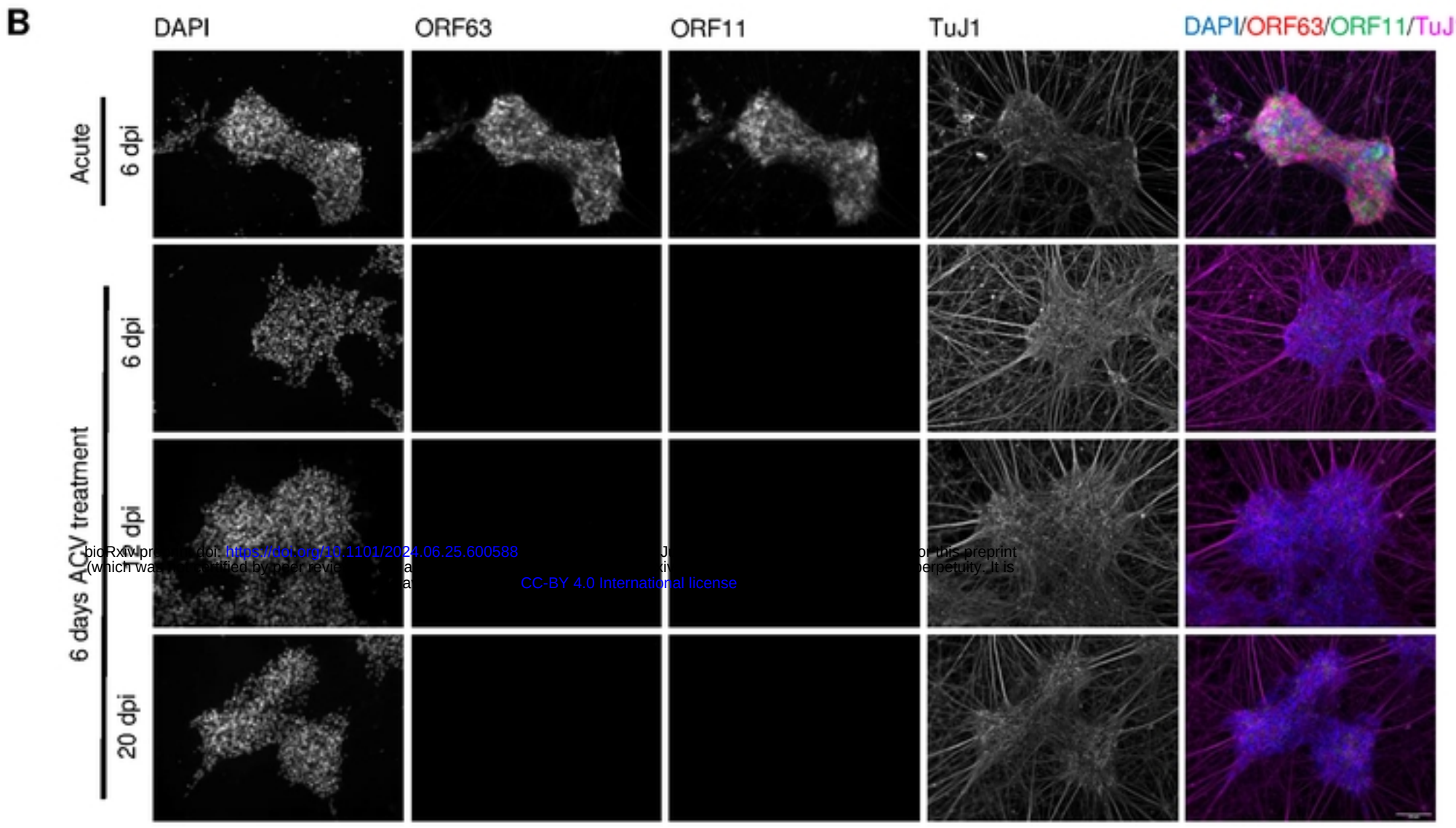

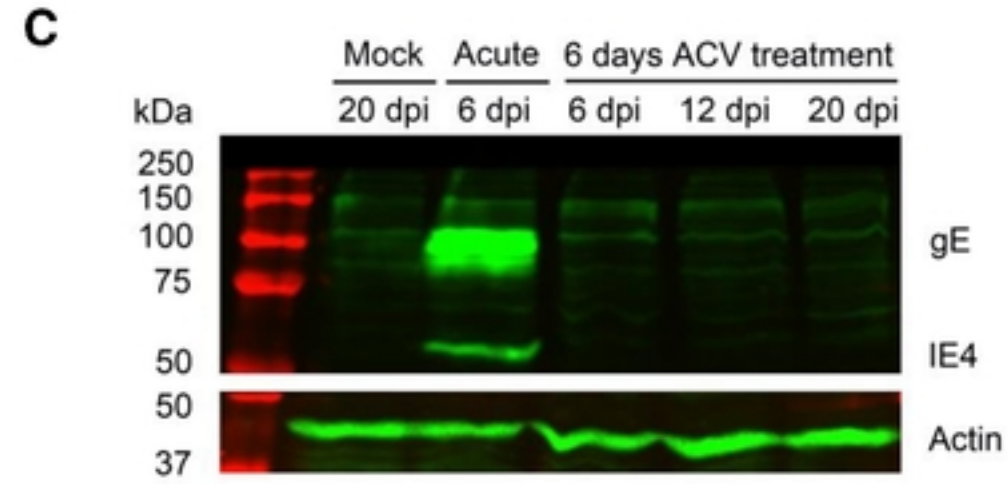

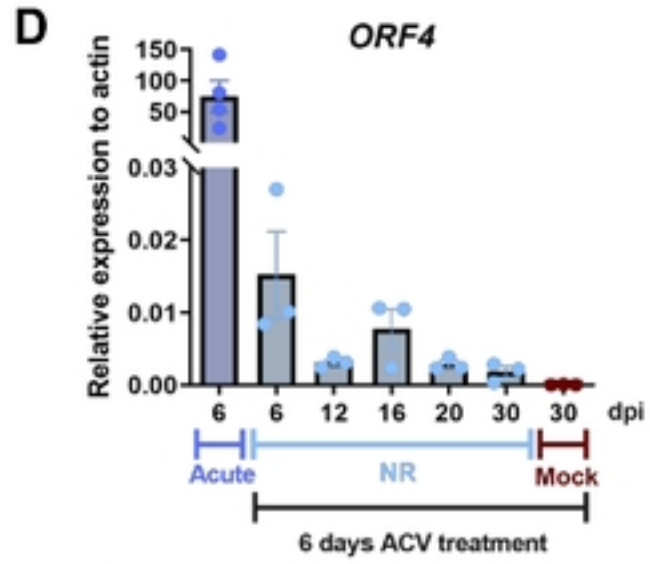

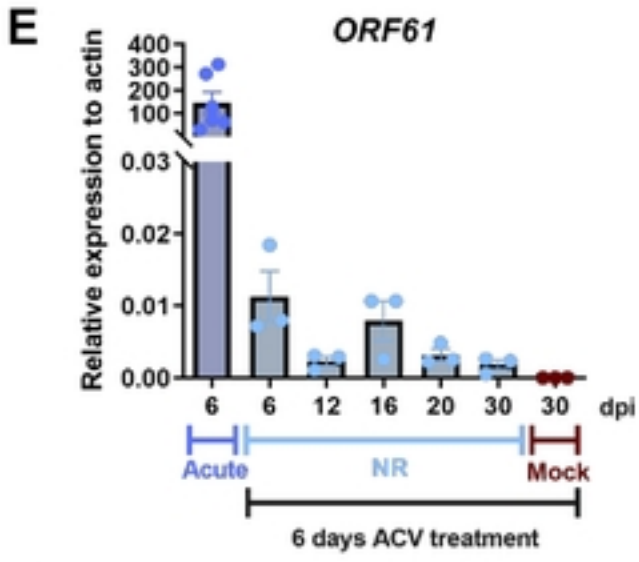

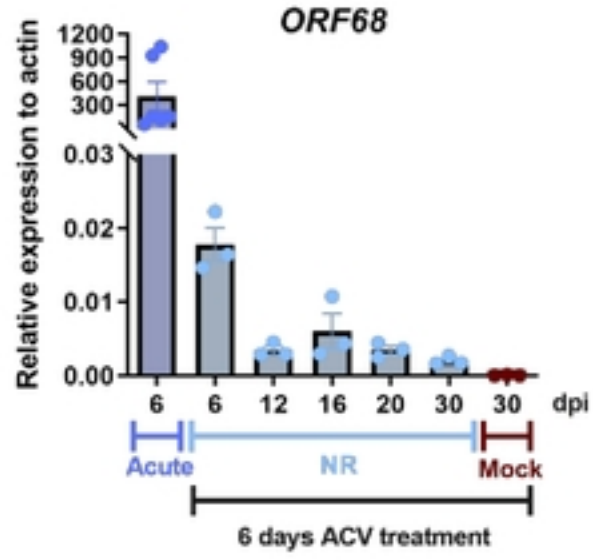

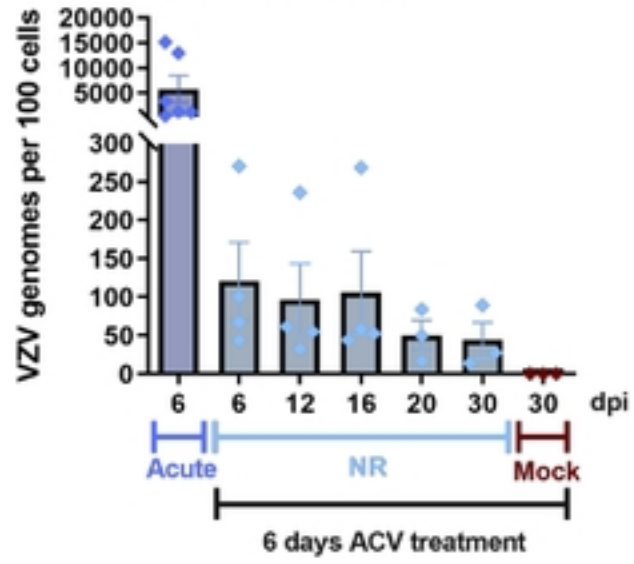

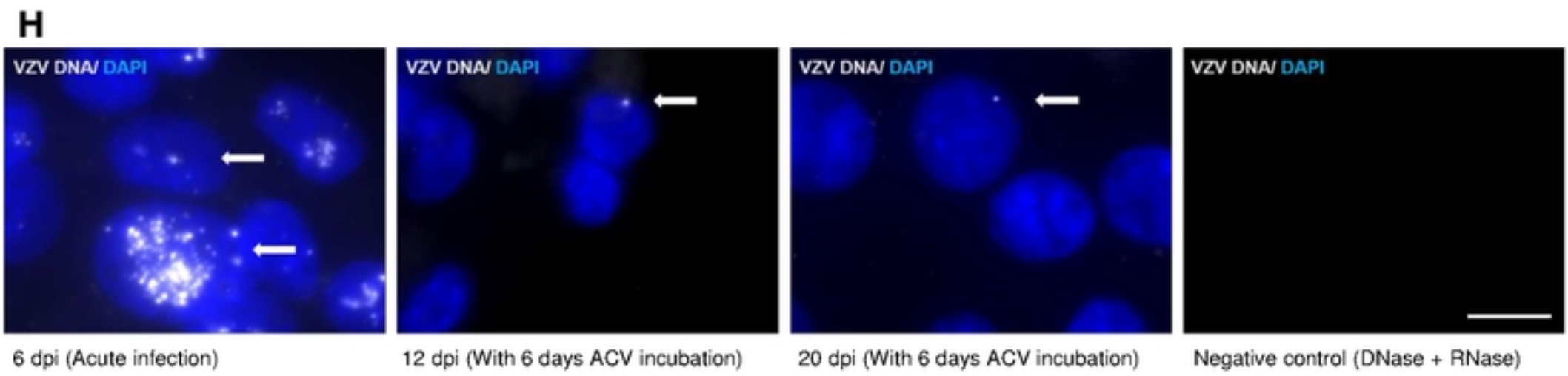

Figure 6

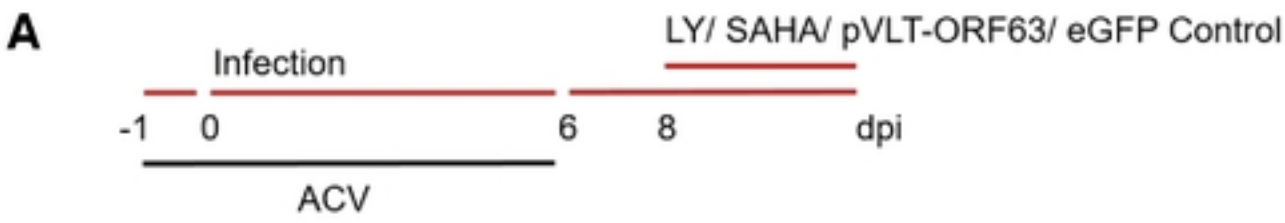

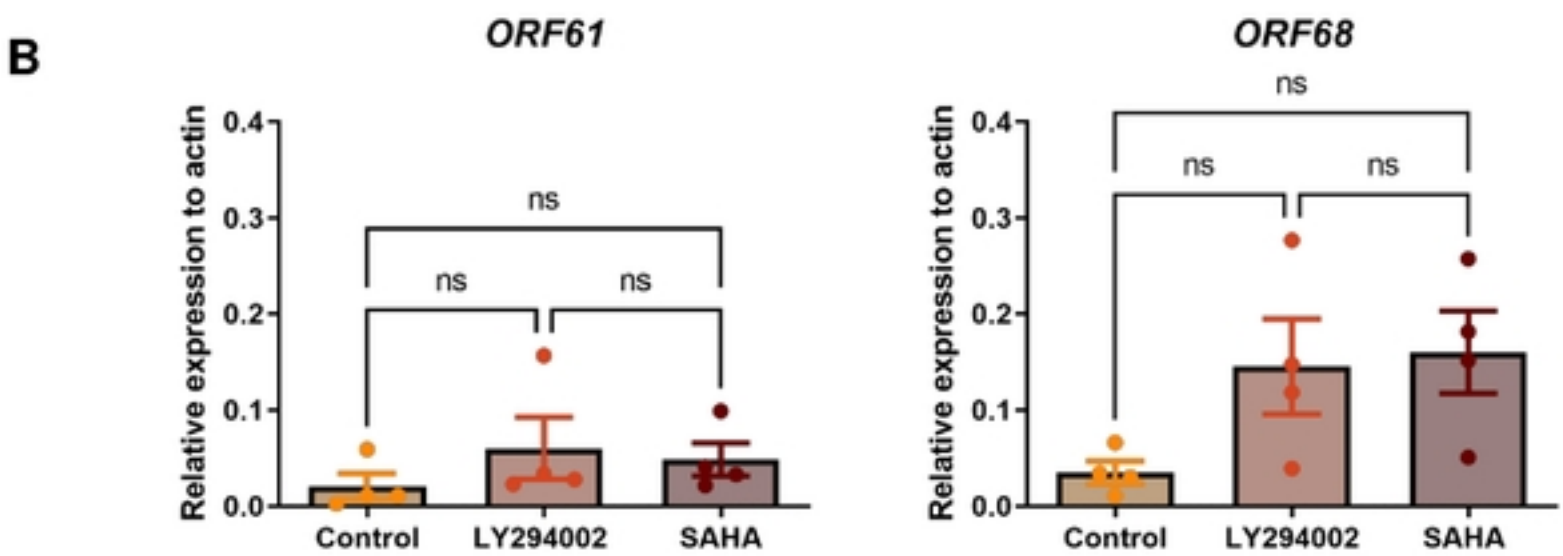

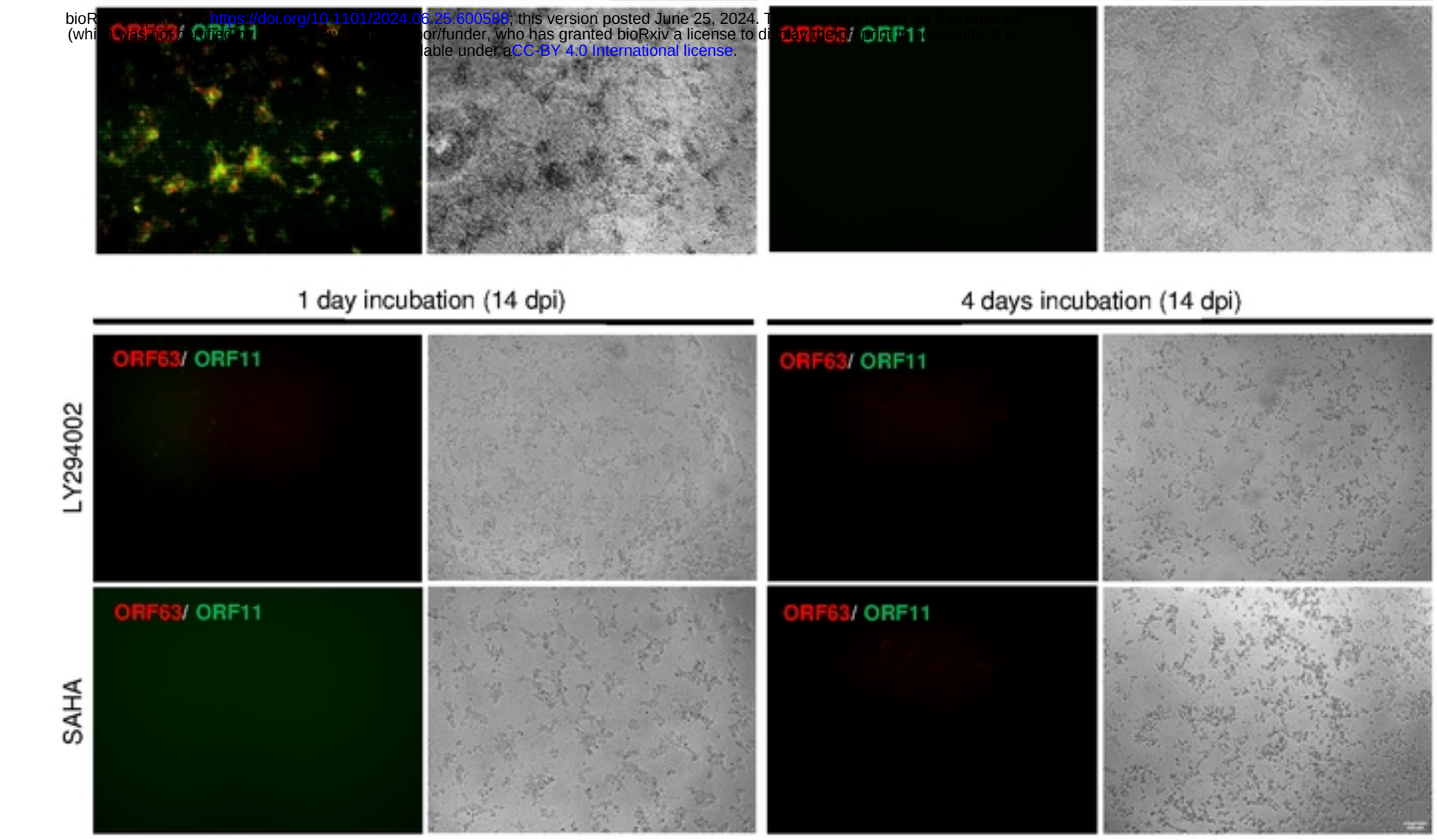

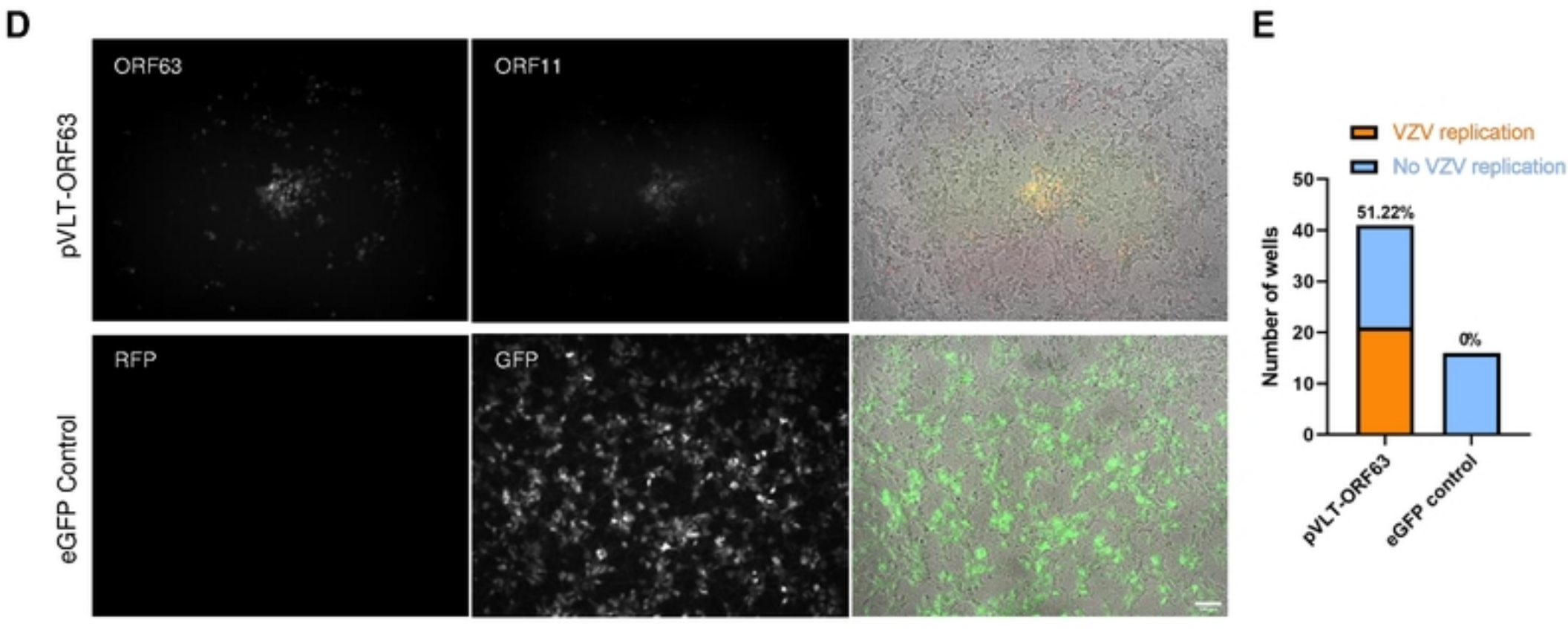

Figure 6

Figure 7

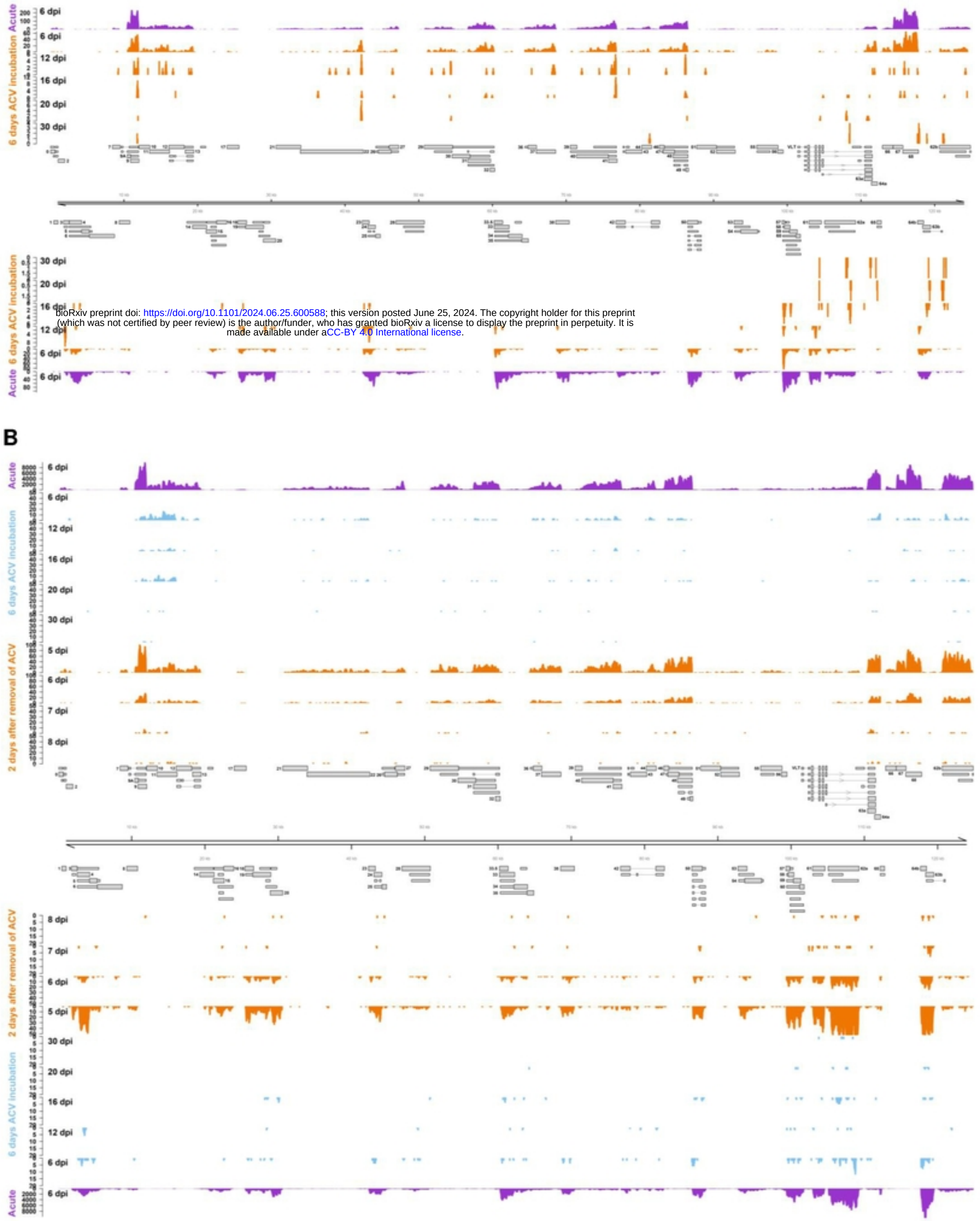

C

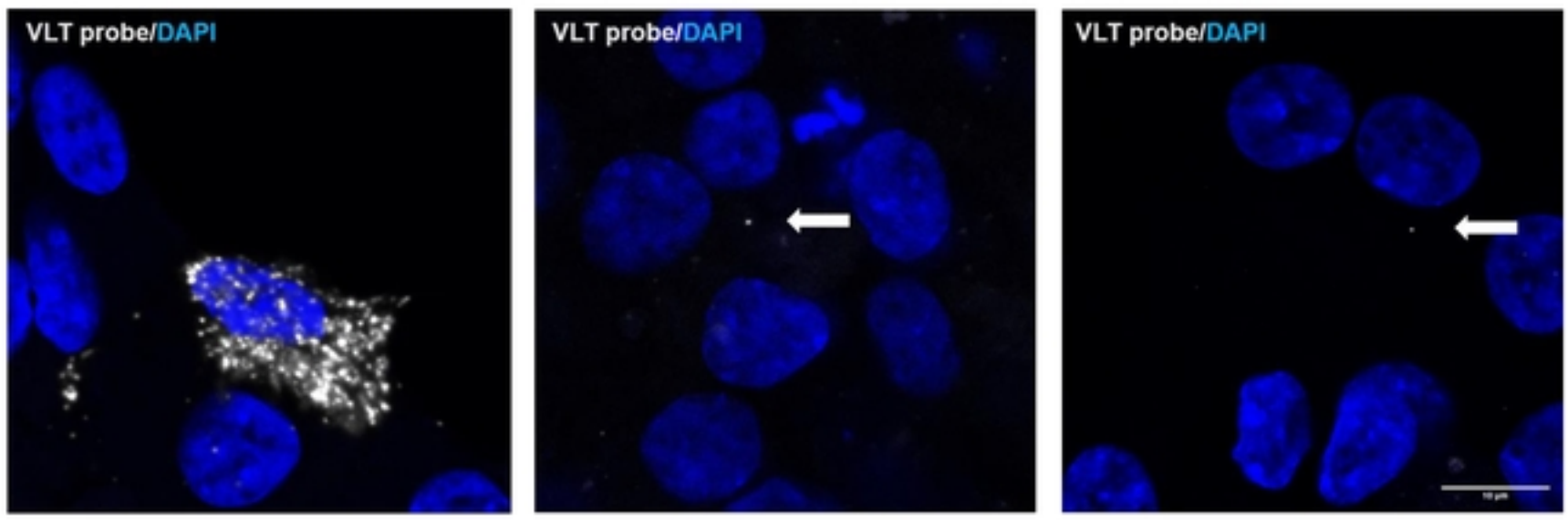

Figure 8

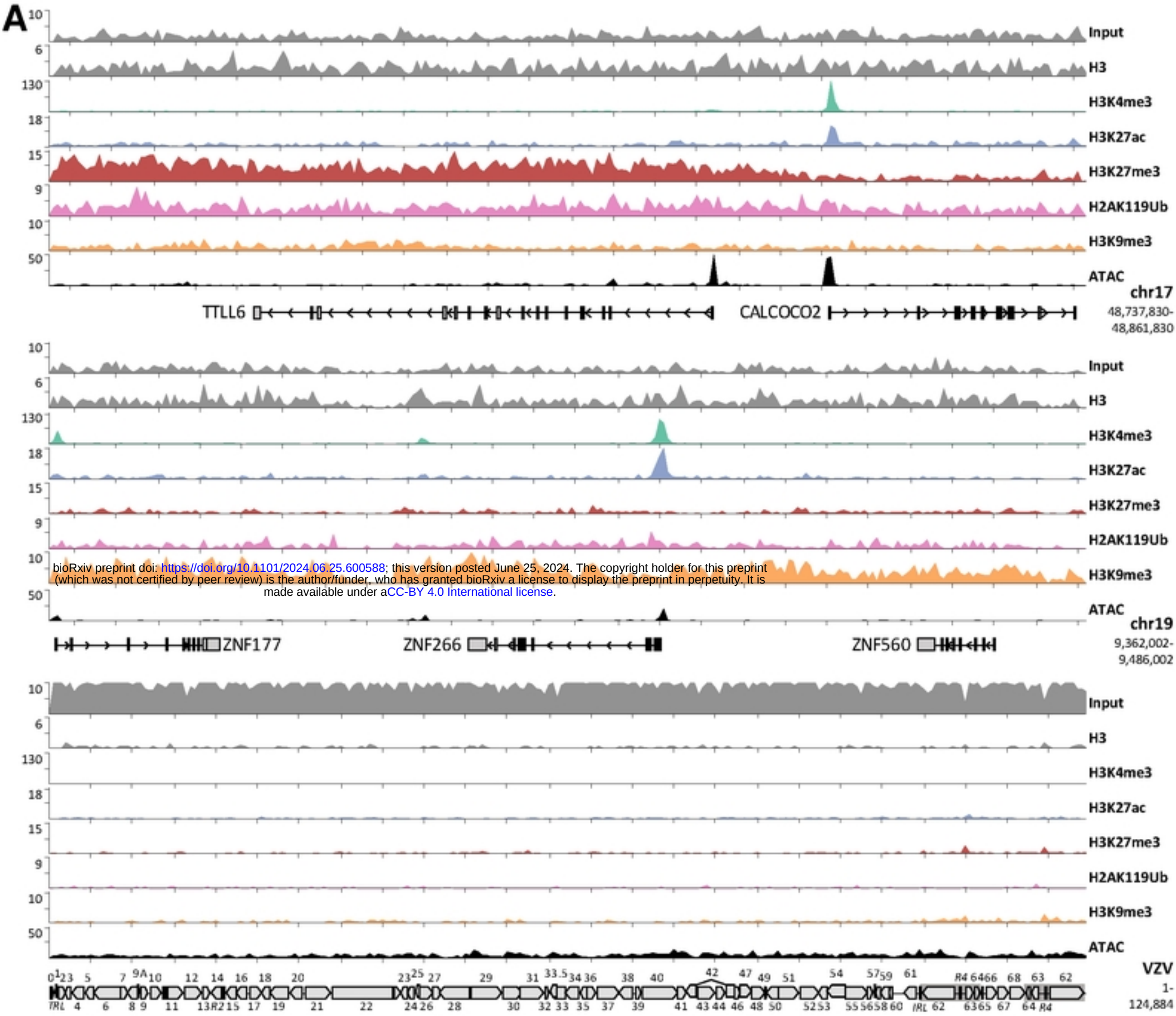

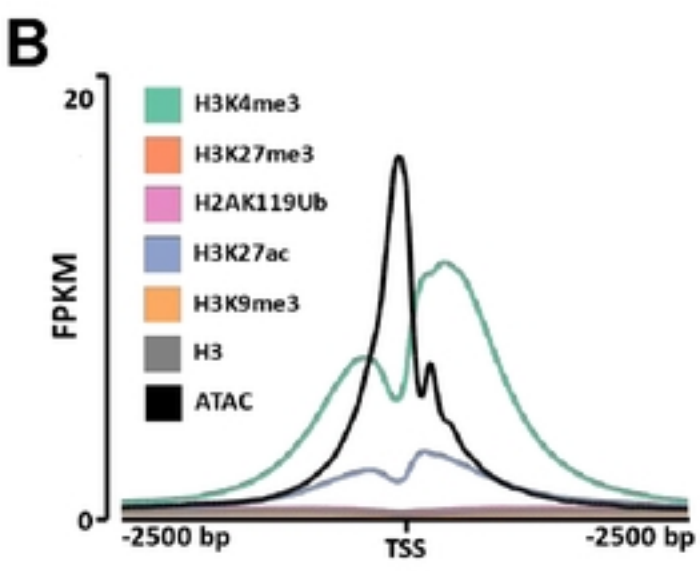

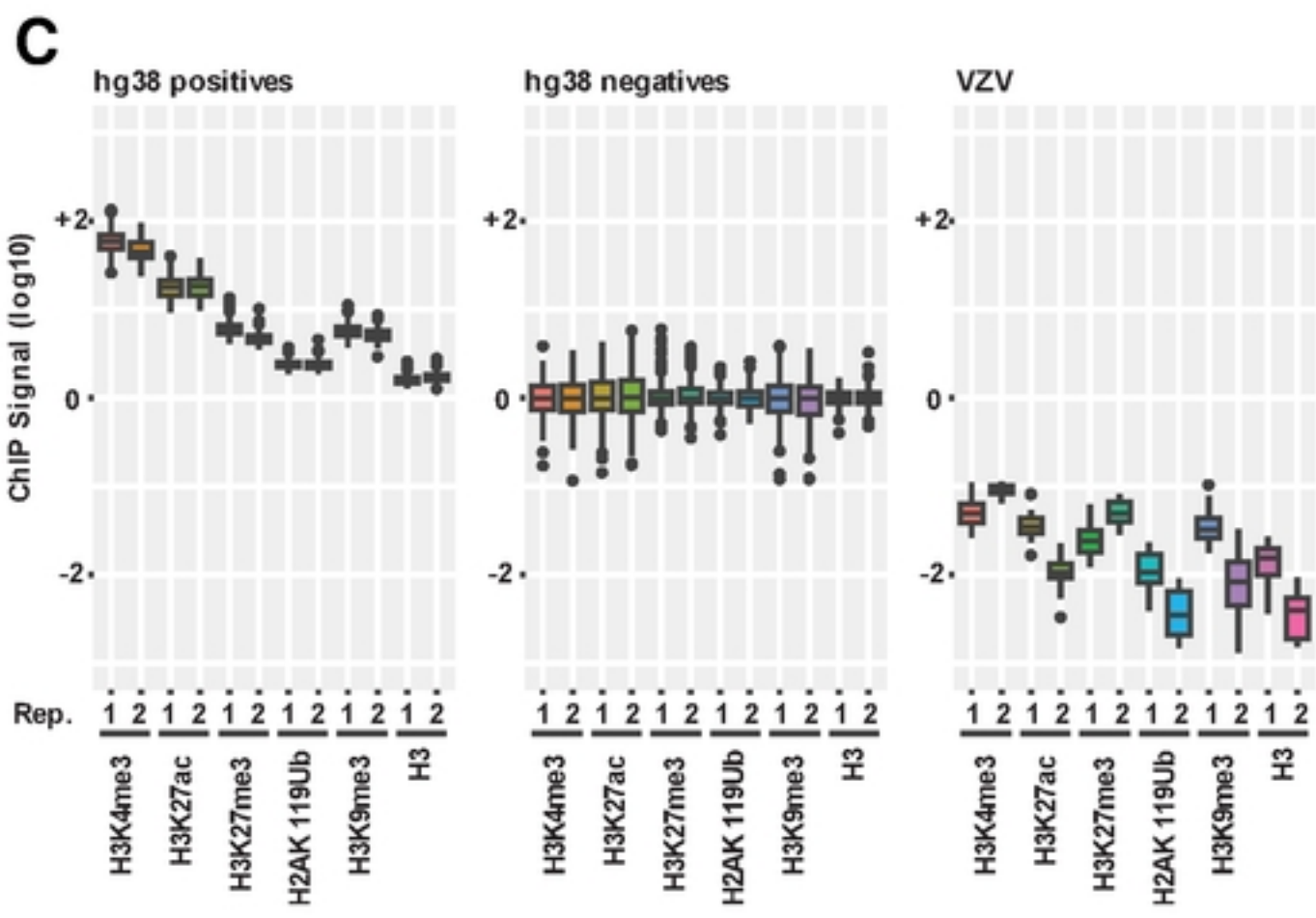

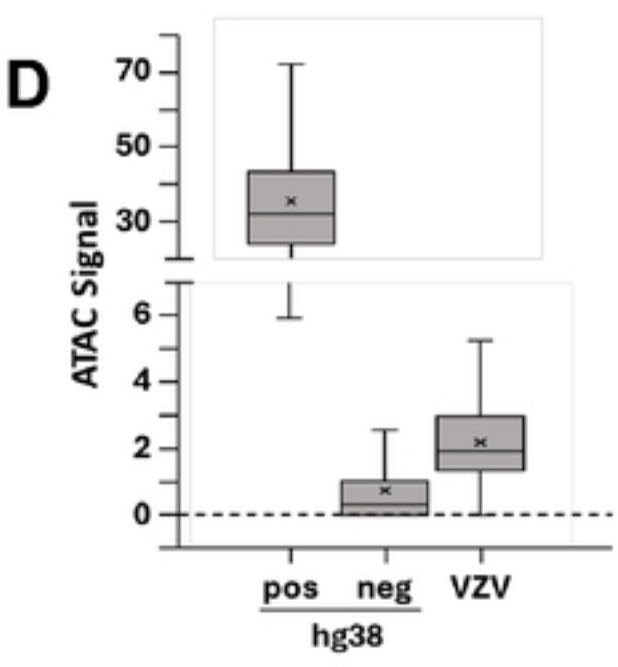

Figure 8